

CHARACTERIZATION OF MULTI-CARRIER LOCATOR PERFORMANCE

by

Daniel E. Breen, Jr.

A Thesis  
Submitted to the Faculty  
of the  
WORCESTER POLYTECHNIC INSTITUTE  
in partial fulfillment of the requirements for the  
Degree of Master of Science  
in  
Electrical and Computer Engineering  
by

---

May 2004

APPROVED:

---

Professor David Cyganski, Major Advisor

---

Professor William R. Michalson

---

Professor R. James Duckworth

## **Abstract**

Time-Difference-of-Arrival (TDOA) location estimation is central to an OFDM based Precision Personnel Locator system being developed at WPI. Here we describe a component of the effort towards characterizing the performance of such a system and verifying the functionality of hardware and software implementations. The performance degradations due to noise in the received signal and misalignments between transmitter and receiver clock and heterodyne frequencies are investigated. This investigation involves development of a MATLAB simulator for the entire system, experimental measures using a prototype implementation and linearized analytic analysis of specific subsystems. The three types of characterizations are compared, confirming agreement, and analytic results are used to demonstrate construction of a system engineering design tool.

## Acknowledgements

There are many people who have contributed to my success here at WPI. To all of them I am grateful.

I would like to thank my parents and entire family for their constant support as I completed college. My friends from UMass-Amherst: Darrin Jacque, Dave Rust, Keith Grimes, Adrienne Brown, Mike Shaw, Scott Foster and Brian Kulig who were always there with encouragement and assistance when needed. My fellow denizens of the Machine Vision Lab: Dave Holl, Nick Hatch, Ben Woodacre, Pavan Reddy, Darius Kazemi and Nick Sherwood. They helped me with my work and made my experience much more enjoyable and easier.

Special thanks to Professor David Cyganski for giving me this research opportunity. His knowledge, guidance and sense of humor made this past year pass very quickly and with a minimal amount of pain. I have learned a great deal while working with him. I would also like to thank Professor Edward Clancy, whose advice helped me shape my Masters degree program and led to my working for Prof. Cyganski. My Thesis Committee: Professors David Cyganski, William Michalson and James Duckworth. Many thanks for their advice and support. Their efforts are the reason my thesis was finished on time.

This research was supported by the U.S. Department of Justice, Office of Justice Programs, National Institute of Justice. I would like to thank them for their support of this work.

Dan Breen

April 2004

# Contents

<b>List of Figures</b>	<b>v</b>
<b>List of Tables</b>	<b>vii</b>
<b>1 Introduction</b>	<b>1</b>
<b>2 Background</b>	<b>9</b>
2.1 System Overview . . . . .	9
2.2 Current Demonstrator System . . . . .	12
2.3 TDOA . . . . .	16
<b>3 RTOA Estimation Performance</b>	<b>18</b>
3.1 A Matlab Simulator . . . . .	18
3.2 Simulation Parameters . . . . .	19
3.3 Calculating Simulation Statistics . . . . .	22
3.4 Analytic Performance Prediction . . . . .	23
3.5 Performance Simulations . . . . .	24
3.6 Nomographs . . . . .	25
3.7 Experimental Performance . . . . .	29
<b>4 Frequency Skew and Shift Effects</b>	<b>33</b>
4.1 Matlab Simulator . . . . .	35
4.2 Simulation Results . . . . .	36
4.3 Analytical Results . . . . .	43
4.4 Experimental Results . . . . .	51
<b>5 Conclusions</b>	<b>52</b>
<b>Bibliography</b>	<b>55</b>

# List of Figures

1.1	Example location scene geometry. . . . .	3
1.2	Transmitter location using TOA. . . . .	4
1.3	Transmitter location using TOA in audio demonstrator. . . . .	5
1.4	Transmitter location curves for distance differences between two receivers. . . . .	6
1.5	Transmitter location using TDOA between three receivers. . . . .	7
1.6	Locator system block diagram. . . . .	7
2.1	The multi-carrier signal . . . . .	10
2.2	Forming the multi-carrier signal. . . . .	10
2.3	Locator system block diagram. . . . .	11
2.4	Audio demonstrator block diagram. . . . .	13
2.5	Current audio demonstrator with four receivers and one transmitter. . . . .	14
2.6	Current audio demonstrator GUI. . . . .	14
3.1	Matlab RTOA performance simulator block diagram. . . . .	19
3.2	The multi-carrier signal . . . . .	20
3.3	General receiver and transmitter geometry. . . . .	26
3.4	Specific receiver and transmitter geometry. . . . .	27
3.5	Energy, bandwidth and vector length nomograph. . . . .	28
3.6	System design example nomograph. . . . .	29
3.7	Instrumented audio demonstrator block diagram. . . . .	30
4.1	Clock synchronized: Amplitude $A$ carriers are captured perfectly. . . . .	34
4.2	Frequency shift: Amplitude $A$ carriers are offset a constant $\delta_\Omega$ . . . . .	34
4.3	Frequency skew: Amplitude $A$ carriers are offset by $n\epsilon$ . . . . .	34
4.4	RTOA estimate with $\pm 0.00001$ freq. skew factor. . . . .	37
4.5	RTOA estimate with $0.00001$ freq. skew factor and $\pm 0.5$ oscillator shift channel fraction. . . . .	38
4.6	RTOA offset as a function of the ratio of $T_x$ and RN clock frequencies (freq. skew factor). . . . .	39
4.7	RTOA offset as a function of local oscillator shift in terms of a fraction of the carrier spacing (oscillator shift channel fraction). . . . .	40
4.8	RTOA estimate with $\pm 0.01008$ freq. skew factor. . . . .	40

4.9	RTOA estimate deviation with $\pm 0.01008$ freq. skew factor. . . . .	41
4.10	RTOA estimate with 0.98992 freq. skew factor and $\pm 0.1$ oscillator shift channel fraction. . . . .	41
4.11	RTOA estimate with 0.01008 freq. skew factor and $\pm 0.1$ oscillator shift channel fraction. . . . .	42
4.12	RTOA estimate with 0.99048 freq. skew factor and $\pm 0.1$ oscillator shift channel fraction. . . . .	43
4.13	RTOA estimate with 0.00952 freq. skew factor and $\pm 0.1$ oscillator shift channel fraction. . . . .	44
4.14	RTOA estimate with $\pm 0.01008$ freq. skew factor. . . . .	44
4.15	RTOA estimate deviation with $\pm 0.01008$ freq. skew factor. . . . .	45
4.16	RTOA estimate with $\pm 0.5$ oscillator shift channel fraction. . . . .	45
4.17	Phase response of first order approximation for $\epsilon = 0.01008$ and $N = 16$ . . .	48
4.18	Phase response of first order approximation for $\epsilon = 0.01008$ and $N = 128$ . .	48
4.19	Phase response of first order approximation for $\epsilon = 0.01008$ , $\delta_\Omega = 0.1$ and $N = 16$ . . . . .	50
4.20	Phase response of first order approximation for $\epsilon = 0.01008$ , $\delta_\Omega = 0.1$ and $N = 128$ . . . . .	50

# List of Tables

1.1	Common abbreviations . . . . .	8
2.1	Audio and RF signal frequencies using the same wavelength. . . . .	15
3.1	Specified simulation parameters . . . . .	20
3.2	Calculated simulation parameters . . . . .	22
3.3	Specified simulation parameters . . . . .	24
3.4	FFT stage simulation and analytic results . . . . .	25
3.5	SSE stage simulation and analytic results . . . . .	25
3.6	Parameters used for experimental RTOA performance results in Table 3.7. .	31
3.7	Experimental Performance Results . . . . .	31
4.1	Specified simulation parameters . . . . .	36

# Chapter 1

## Introduction

This thesis effort supported a multi-team research project in which an indoor/outdoor geolocation system, called the Precision Personnel Locator (PPL), was being developed. The PPL was designed as a means to provide a deployable geolocation system to help track first responders in an unknown environment. As personnel move around the area of interest, the transmitter that each person carries emits a signal that is used by receivers to locate each transmitter. An important future enhancement to the locator system will be the ability to generate a map of the operations area as the personnel move around. This map, coupled with personnel tracking, would allow personnel monitoring everyone's movements from outside to direct people to an exit in the case of low visibility, when the original entry point is unaccessible or when the person becomes disoriented.

The PPL system was designed for first responders who have a need for tracking each other at the location to which they were called. The area of interest could contain an individual building or a larger area with perhaps a mixture of buildings, various structures and open spaces. The wide range of possible environments necessitate a locator system that is easily deployed, adaptable to any environment and quick to deploy and configure. Multi-path reflections will be a problem inside buildings, so the system will have to be able to determine the direct-path solution and ignore false signals due to reflections which may be strong. The locator system should also be quick and easy to set up, since minimizing the deployment and configuration time is important since that allows personnel to concentrate

on their primary job.

When the first responders arrive on the scene, they will have to deploy the locator infrastructure as none can be assumed as pre-installed. Reference Nodes (RNs) will be placed in fixed locations around the perimeter of the work area. The RNs will determine the distances between each other via an exchange of signals similar to what the mobile transmitters will broadcast. The set of inter-reference node distances can be used to determine the reference node's spatial relationship and establish a coordinate system in which the transmitter positions will be determined. Once the reference node's relative positions are established, location solving can commence. Each RN calculates a relative time-of-arrival (RTOA) for each transmitter in the field. The time-difference-of-arrivals (TDOAs) will be determined by out-of-band collaboration between the RNs. One of the reference nodes, acting as the control unit, will determine each transmitter's location in the coordinate system using the TDOA set and RN positions.

An example of one possible operational scene is shown in Fig. 1.1. In this scenario, firefighters and possibly other first responders are to be tracked inside the building. Reference nodes are located on each fire truck which have parked alongside two sides of the building. Each truck has two RN pairs on board which are located at each end of the truck. Each RN pair consists of one RN at the base with the other located some distance above the base node. One of the nodes has been chosen as the control unit and all the reference nodes conduct their inter-node communication via an 802.11 side channel. Each RN uses the side channel to send TOA estimates for each transmitter to the control unit for location estimation. As personnel make their way through the building, their movements are tracked and displayed. If anyone becomes disoriented or lost, the person monitoring the locator display outside will be able to provide a current location and directions out of the building. If someone were to become incapacitated or trapped, their current location would be known and rescue teams could be directed to that position.

This locator uses fixed-position receivers to precisely estimate the location of moving transmitters. Together, the receivers establish an ad-hoc coordinate system and self-synchronize their clocks with each other, while each transmitter's clock is asynchronous with respect to other transmitters and the receivers. Each receiver processes the received signal

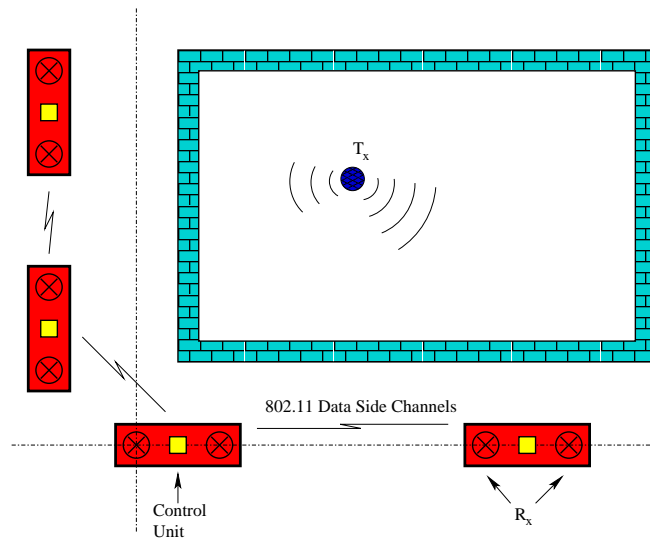


Figure 1.1: Example location scene geometry.

and uses a State-Space Estimator (SSE) to estimate the relative time-of-arrival (RTOA) for the signal with respect to an arbitrary reference time. All the RTOAs are combined to obtain a set of well-known time-difference of arrivals (TDOAs). A location estimation algorithm uses the TDOA set and the receiver locations in the established coordinate system to determine the location of each transmitter.

For purposes of introduction to the location solution problem consider the fact that location solving can be easily performed using true TOAs where a true TOA can only be computed if transmitters and receivers share synchronized clocks. Using the speed of light, each TOA can be converted into a distance that represents how far the RN is from the transmitter. This distance represents the radius of a circle centered on the corresponding RN indicating a locus of possible transmitter locations given that single piece of data. The intersection of these circles indicates the transmitter's possible location. In a 2-D system, three RNs are needed to find an unambiguous position solution since using only two RNs yields two solutions. In general a total of  $n + 1$  RNs are necessary for location in  $n$ -dimensional space when TOAs are used. Fig. 1.2 shows a 2-D position estimation using three RNs with the distance from each TOA forming a circle centered on the respective RN. Notice that if one of the RNs were eliminated, there would be two possible position solutions,

one corresponding to the actual transmitter position and the other a false solution.

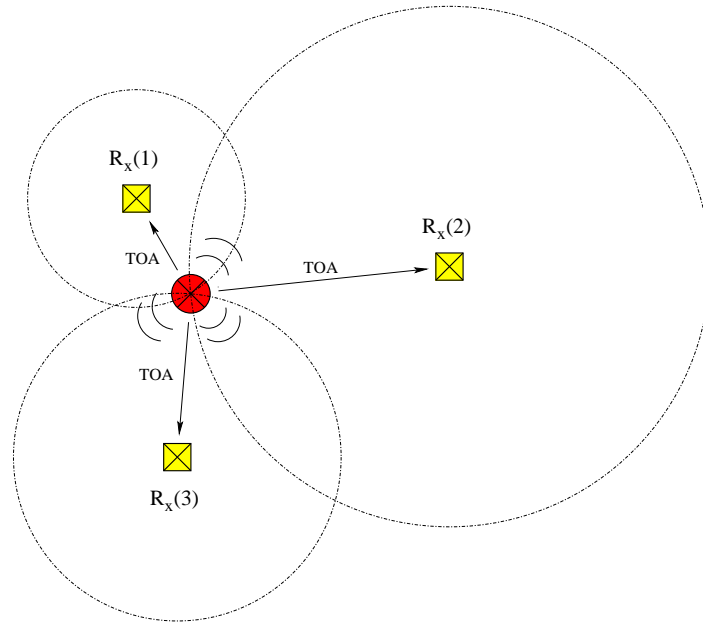


Figure 1.2: Transmitter location using TOA.

An early version of our "audio demonstrator system" (described in detail in Sec. 2.2) performed location from TOAs with two receivers. The audio demonstrator system is a locator system used to develop the software and hardware technology needed for a full-scale system. Audio signals are used for location in this system rather than RF. Fig. 1.3 is a screen capture of the demonstrator's position display. The two receivers are displayed in their fixed positions as small crosses. The straight line connecting the two receivers is where theoretically only one position solution is possible since the two TOA circles would intersect at one point only. The two transmitter positions are the circumscribed crosses. In this case the lower right transmitter position is the correct solution and the upper left solution is incorrect. The next version of this demonstrator still used TOA for location, but added a third receiver to eliminate the incorrect solution.

While TOAs alone can be used for position solving, they are only available when the transmitter and RN clocks are synchronized. When the transmitter and RN clocks are not synchronized a time offset,  $\tau_d$  is introduced into the TOAs hence our RTOA nomenclature.

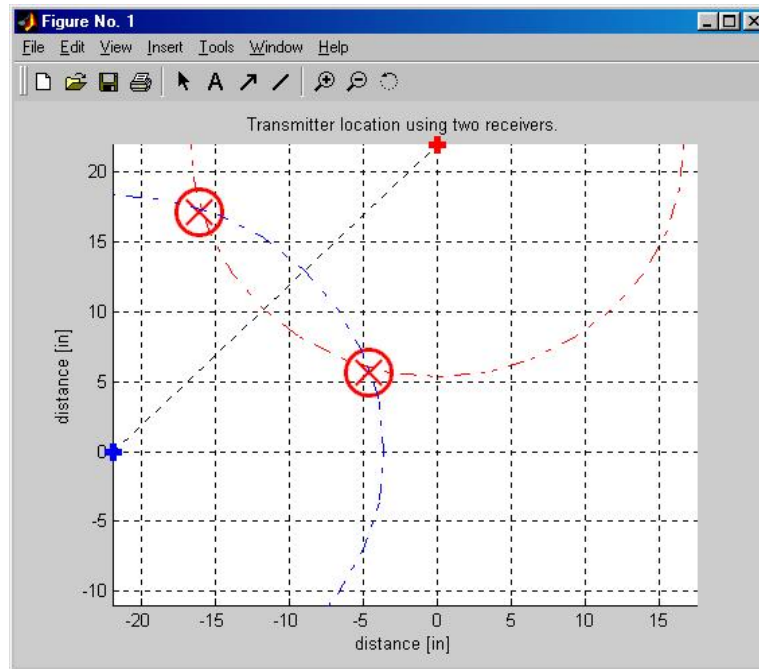


Figure 1.3: Transmitter location using TOA in audio demonstrator.

This time offset will be the same for all RNs if they are clock synchronized with each other. In order to eliminate the time offset,  $\tau_d$ , TDOAs are calculated from the RTOA estimates. Taking the difference between two RTOAs subtracts out  $\tau_d$  since it is the same at all receivers. When the locus of possible transmitter locations for a given TOA is plotted, it takes the form of a circle, centered on the RN, with a radius equal to the distance between transmitter and receiver. TDOAs, on the other hand, give rise to transmitter position loci in the form of a hyperbola located between two RNs. The actual transmitter location will be located somewhere on the hyperbola. Fig. 1.4 shows TDOA curves for various distance differences,  $\delta$ , between two RNs. The difference distance,  $\delta$  is calculated from each TDOA using the speed of light relationship.

$$\delta = c \cdot TDOA$$

In the example shown in Fig. 1.4, one RN is located at the origin and the other is located on the x-axis at 1 m. The vertical line at 0.5 m is the locus for which  $\delta = 0$ . When the

TDOA is positive, the hyperbola is centered around the RN to the right of the  $\delta = 0$  line and when the TDOA is negative the hyperbola is centered around the RN to the left of the  $\delta = 0$  line. Location in  $n$ -dimensional space utilizing TDOA information requires  $n + 1$  RNs, therefore three RNs are necessary for 2-D location. For example, Fig. 1.5 shows 2-D location with  $RN_0$  at the origin,  $RN_1$  is 1 m away along the positive x-axis and  $RN_2$  is 1 m away along the positive y-axis. In this example  $\delta_{01} = 0.1$  m and  $\delta_{02} = 0.8$  m. The transmitter is located at the intersection of the two hyperbolae.

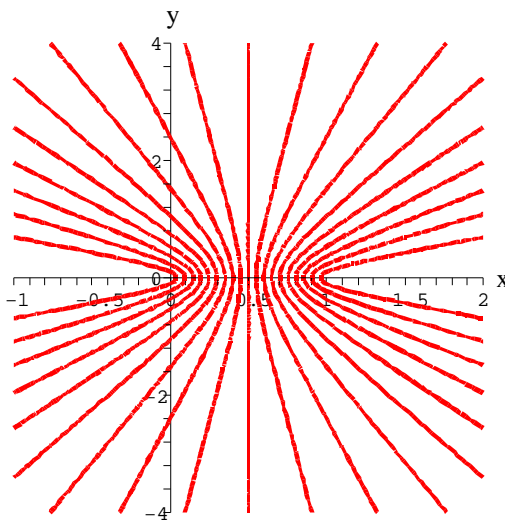


Figure 1.4: Transmitter location curves for distance differences between two receivers.

This thesis examines RTOA estimation in the presence of performance degraders. The three performance degraders considered are additive white Gaussian noise (AWGN), frequency skew between receiver and transmitter sampling clocks and frequency offset between receiver and transmitter heterodyne oscillators. Figure 1.6 shows a block diagram of our model system with the performance degrader sources. Our methodology for examining RTOA performance in the presence of degraders is as follows. First, a Matlab RTOA performance simulator is described and results presented. Next, analytical performance results are compared to the simulation performance. Finally, our experimental locator demonstrator is then used to provide experimental confirmation of the theoretical results. The analyt-

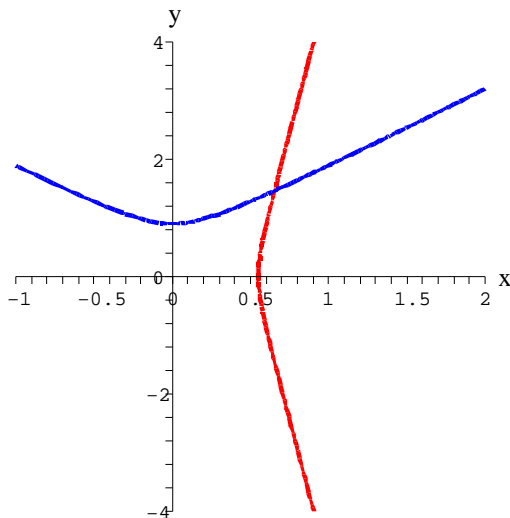


Figure 1.5: Transmitter location using TDOA between three receivers.

ical expressions were then used to develop nomographs relating system energy, fractional bandwidth and sensor array size to locator performance.

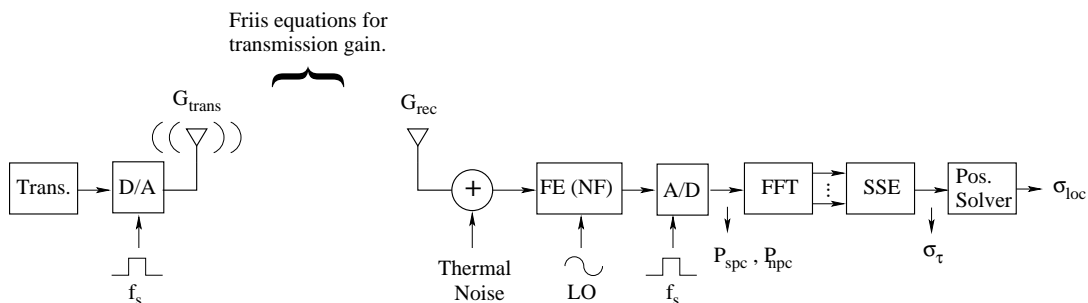


Figure 1.6: Locator system block diagram.

This thesis is organized as follows: Chapter 2 presents an overview of the locator system. Our current audio demonstrator system is also discussed along with TDOA for location. In Chapter 3 RTOA estimation performance results are presented. A Matlab RTOA performance simulator is described with simulation results compared against predicted analytical predictions, the Cramer-Rao bound (CRB) and confirmed experimentally. Additionally

location error equations for a specified geometry are presented and used to generate a nomograph for assisting with system design. A design example using the nomograph is discussed. The effects of frequency skew and shift on RTOA estimation are discussed in Chapter 4, and simulation results are compared to analytical and experimental results. Finally our results are summarized in Chapter 5. There are a few topics mentioned in this thesis for which complete developments are not discussed. In particular, the problems of receiver synchronization, receiver position establishment and solving transmitter location from TDOAs are not discussed since these all belong to the thrusts of team members and will appear in other reports and theses.

Also, this thesis uses several abbreviations and defines many of them only once. Table 1.1 lists these abbreviations for the reader's convenience.

PPL	Precision Personnel Locator
TOA	Time of Arrival
RTOA	Relative Time of Arrival
TDOA	Time Difference of Arrival
SSE	State Space Estimator
CRB	Cramer-Rao Bound
RN	Reference Node
OFDM	Orthogonal Frequency Division Multiplexing
AWGN	Additive White Gaussian Noise
FFT	Fast Fourier Transform
IFFT	Inverse Fast Fourier Transform

Table 1.1: Common abbreviations used throughout this thesis.

## Chapter 2

# Background

### 2.1 System Overview

In our Precision Personnel Locator (PPL) system, independent, mobile transmitters continuously transmit an Orthogonal Frequency Division Multiplexing (OFDM) signal (Fig. 2.1) that is received by multiple receivers located in arbitrary, fixed locations. The OFDM transmitted signal is constructed from  $N$  equally spaced sinusoidal components in the frequency domain to form an  $N$  channel signal. The amplitude coefficients of the sinusoids are chosen such that the signal consists of  $M$  carriers spaced  $K$  channels apart with the first carrier at channel  $Fb$ . We define channel frequency spacing as  $\delta_f$  and carrier frequency spacing as  $\Delta_f$ . The signal amplitude coefficient vector specifying this signal may be passed through an  $N$ -point Inverse Fast Fourier Transform (IFFT) to obtain the  $N$  time samples needed to generate the time waveform to be transmitted. Conceptually, the IFFT result may be serialized after which the time samples are realized by the digital-to-analog (D/A) converter at sampling frequency  $f_s$  yielding a  $T = \frac{N}{f_s}$  second period, periodic, analog transmitted signal. A more economical implementation would involve storing the waveform samples in a read-only memory which is cyclically read to obtain the sample values as needed. Fig. 2.2 shows the signal generation process used. During the initial system configuration, the receivers communicate to establish relative position information about each other, build a coordinate system and synchronize their system clocks.

Once the initial configuration procedure is finished, transmitter location estimation can begin. Fig. 2.3 shows the basic components of the locator system. Each mobile transmitter is comprised of a waveform generator feeding a power amplifier with the  $T$  second period signal, continuously transmitting through an omni-directional antenna. The signal is received via another omni-directional antenna and processed through the front end of the receiver. Every  $N$  sample data set is then stored in a buffer for further processing.

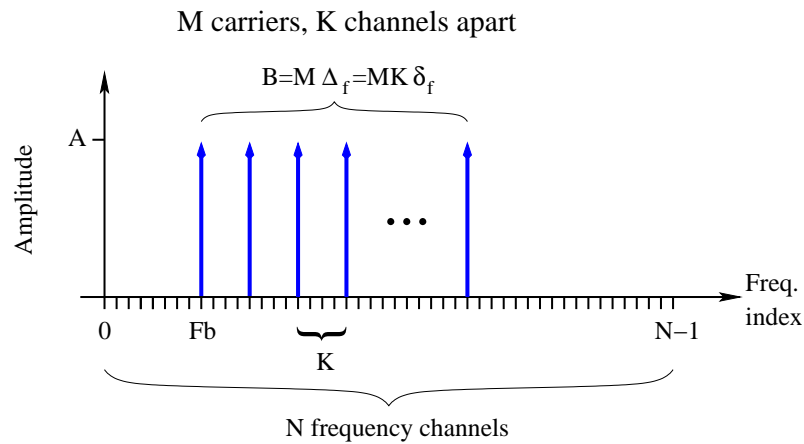


Figure 2.1: The multi-carrier signal

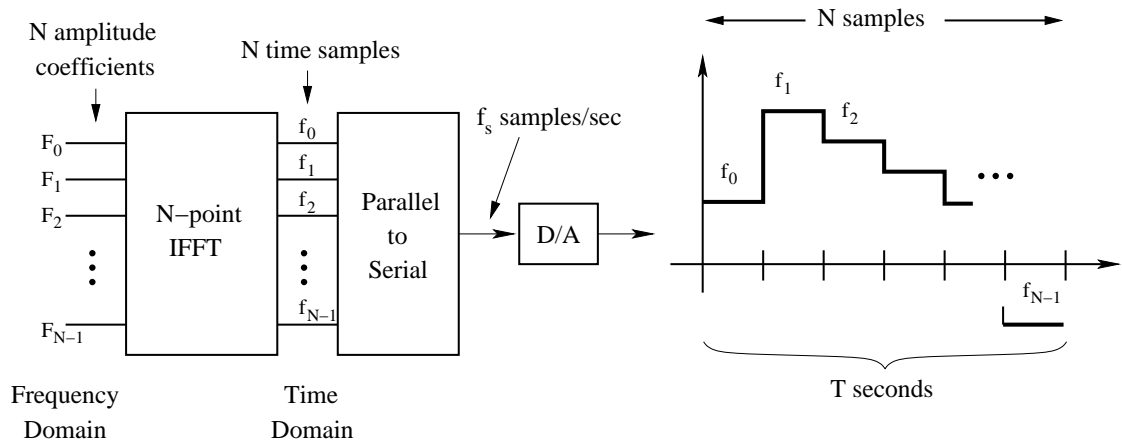


Figure 2.2: Forming the multi-carrier signal.

Each  $N$  sample data vector is first passed through an  $N$ -point Fast Fourier Transform

(FFT), after which the carrier data is isolated and a preset phase correction performed. Next the carrier data is processed by the state space estimator (SSE) [2] which generates phase-magnitude pairs, that are converted into RTOA estimates using the carrier spacing,  $K$  and the sampling frequency  $f_s$ . This process is typical for all receivers in the locator system. The RTOA estimates from each receiver are exchanged through a side channel and the TDOA matrix is formed from the RTOA set. Finally the TDOA matrix and receiver location information is used by the position solver to determine the current transmitter location. This process is continuously repeated and each location estimate displayed in real-time.

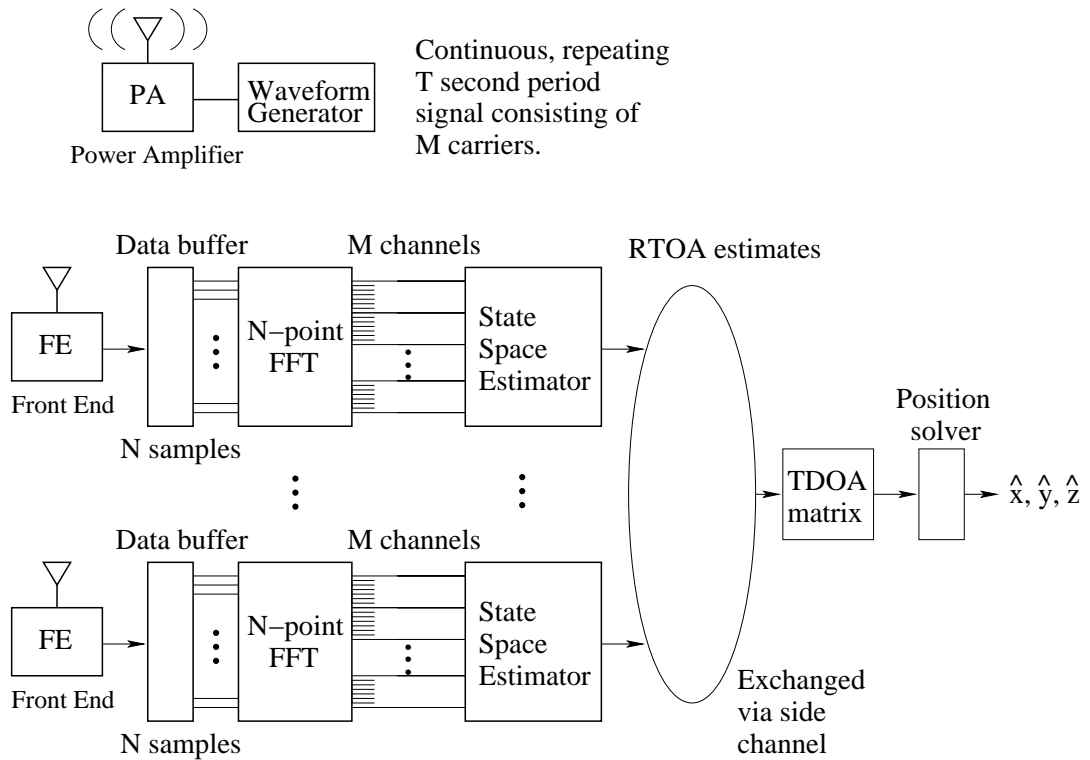


Figure 2.3: Locator system block diagram.

## 2.2 Current Demonstrator System

An audio demonstrator system was built as a proof-of-concept and to act as a test bench for developing the software necessary for the RF location system. Since audio signals are used, the transmitter is a small speaker coupled with an audio amplifier and the receivers are microphones. Fig. 2.4 shows a block diagram of our audio demonstrator. Our multi-carrier signal is generated on the laptop computer using Matlab and continuously delivered to the transmitter via a National Instruments data acquisition (NiDAQ) card plugged into the laptop's PCMCIA port. The transmitted signal, received at each microphone, undergoes an A/D conversion in the NiDAQ and is buffered as N-sample blocks. A matrix of N-sample blocks from each receiver is assembled and passed to Matlab for location estimation.

The current version of the audio demonstrator (Fig. 2.5) uses four audio microphones for the receivers and one audio speaker for the moveable transmitter. The receivers and transmitter are connected to a NiDAQ box (upper right of Fig. 2.5) which is connected to the laptop (not visible). Transmitter and receivers are clock synchronized at this time. Each microphone is mounted, face up, at the base of an acrylic tube that makes the directional microphone behave like an omnidirectional receiver. An inverted metal cone is mounted above the speaker to reflect the transmitted signal horizontally. Receiver positions were measured so that true TOAs can be determined from which the TDOAs are calculated for location estimation. The multi-carrier signal consists of  $M = 101$  carriers, spaced  $K = 10$  channels apart, starting at channel  $Fb = 400$  in a  $N = 8192$  sample signal vector. With a sampling frequency of  $f_s = 44100$  Hz, the signal has a bandwidth of 5.383 kHz, centered at 4.845 kHz and occupies a frequency range of 2.153 – 7.537 kHz.

In order to reduce the time involved with setting parameters in the Matlab functions and allow others, less familiar with the software, to easily configure and use the locator, I designed and programmed a GUI in Matlab. Our GUI provides a front-end for the locator system that simplifies configuration and operation. The right half of the GUI window (Fig. 2.6) provides a visual display of the location area. Each receiver location is represented by a blue star and the current transmitter location by a red cross. As the locator system executes, the current position is updated in real-time. For troubleshooting purposes,

signal phase and magnitude can be displayed for any receiver. Text display options include current estimated transmitter location coordinates, estimated receiver-transmitter distances and location statistics (as described in Sec. 3.7). Another useful visual troubleshooting aid converts each RTOA into a distance and displays the corresponding circle around the appropriate receiver. This can be very useful for determining if a receiver is malfunctioning. All experimental tests were performed using this audio demonstrator system.

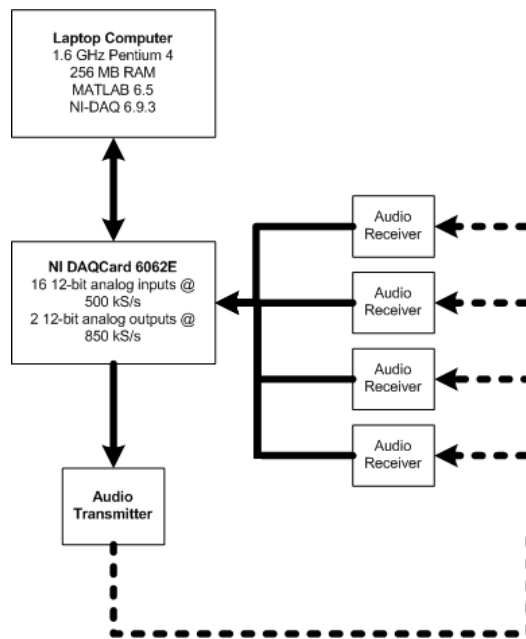


Figure 2.4: Audio demonstrator block diagram.

Our audio demonstrator was designed as a to-scale proof-of-concept for an RF location system. Instead of transmitting and receiving the signal at RF, an audio frequency range of 2.153 – 7.537 kHz was used, which is a 5.383 kHz bandwidth centered around a 4.845 kHz center frequency. The speed of sound in air has a standard value of 1.3047E4 in/sec. Since that value is affected by temperature, humidity and ambient noise, a precise sound velocity was determined experimentally for the specific environmental conditions of a given time and place on those occasions such precision was required. On those occasions we used the audio demonstrator to collect TOA estimates for two positions separated by a fixed distance of 6 in. Subtracting the mean TOA estimate for the two positions gave the TOA between the

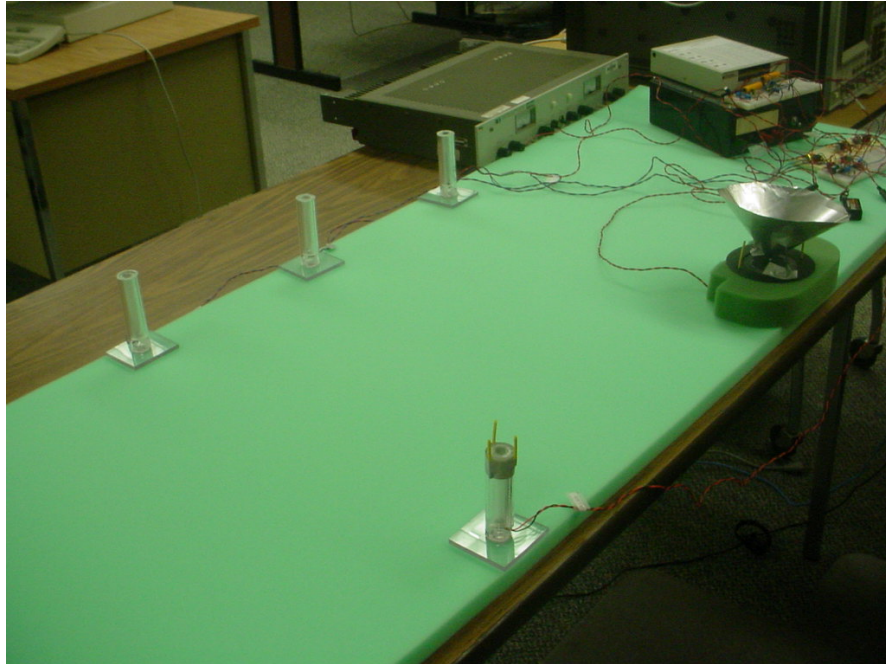


Figure 2.5: Current audio demonstrator with four receivers and one transmitter.

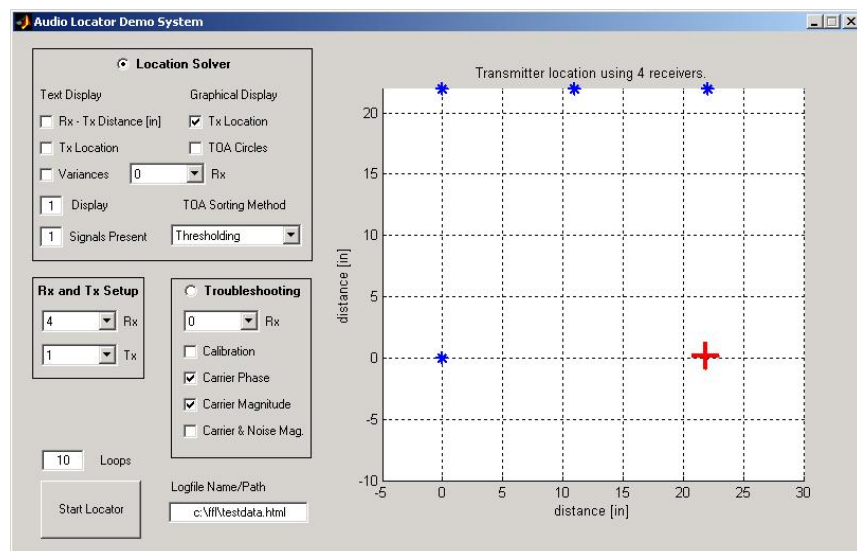


Figure 2.6: Current audio demonstrator GUI.

two positions. Dividing the true distance by the TOA estimated for that distance yielded a measured sound velocity of 1.34E4 in/sec for example on a specific occasion. Dividing our audio frequency range by the measured sound velocity results in wavelengths in air of 6.232 in. and 1.780 in. respectively. Those wavelengths correspond to a RF frequency range of 1.894–6.630 GHz or a 4.735 GHz bandwidth centered at 4.262 GHz. Therefore, the location software developed for the audio demonstrator can be used for an RF location system also. Table 2.1 summarizes the audio signal frequency characteristics and the corresponding RF signal frequency characteristics.

	$f_{min}$	$f_{max}$	BW	$f_{center}$
Audio	2.153 kHz	7.537 kHz	5.383 kHz	4.845 kHz
RF	1.894 GHz	6.630 GHz	4.735 GHz	4.262 GHz

Table 2.1: Audio and RF signal frequencies using the same wavelength.

The audio locator system does a good job of estimating the transmitter position in a location area of about 4 ft. by 6 ft. Location area was partially determined by the size of the table used but it is limited by the spatial ranging cell size,  $R$ .

$$R = \frac{1.3418E4 \text{ in/sec}}{53.833 \text{ Hz}} = 20.77 \text{ ft.}$$

where 53.833 Hz is the carrier frequency separation and 1.3418E4 in/sec is our measured sound velocity. Outside the ranging cell our TDOA estimate is no longer unambiguous due to spatial aliasing[3]. Matlab calculates a new location estimate about once every 186 ms so that the displayed location updated frequently enough that transmitter movement appears to be smooth on screen. There is a option in our software for controlling how often the display is updated which reduces the load caused by Matlab’s display functions. This was introduced when we discovered the updating overhead for the display could cause our data processing to fall behind real time.

Performance results from this system are shown in Table 3.7 and described in Sec. 3.7. All experimental results presented are for the 2-D demonstrator system but some experimentation has been conducted with a 3-D version. Development and testing took place almost exclusively on a 2-D audio location system to reduce testing complexity and avoid

problems caused by the directionality of the receivers and transmitter in 3-D arrangement. The software was designed for 3-D location so that the only modification made for 3-D tests was to add a fifth receiver mounted above the plane of the other receivers. A few test runs confirmed that the transmitter's location was approximately correct but our current transmitter and receiver hardware only allow for a rough functionality confirmation due to the directionality problems mentioned above.

## 2.3 TDOA

While this thesis is concerned with RTOA performance, the locator system relies on TDOAs that are formed from the estimated RTOAs. TDOAs allow us to locate transmitters that are not clock synchronized with the receivers. The lack of clock synchronization between transmitter and receiver adds a time shift in the received signal. However, because the receivers are clock synchronized, that time shift is the same at each receiver. Therefore taking the TDOA between receivers eliminates that time shift. For example, let's take a system where there is one transmitter and two receivers. If the transmitter sends a pulse at time  $t_0$ , receiver 1 will see the pulse arriving at time  $t_1$  and similarly receiver 2 will see the pulse arriving at time  $t_2$ . The time at receiver 1 can be expressed as

$$t_1 = t_0 + t_{01} + \tau_1, \quad (2.1)$$

where  $t_0$  is the time the pulse was transmitted according to the transmitter's clock,  $t_{01}$  is the travel time for the pulse between the transmitter and receiver. The lack of synchronization between transmitter and receiver 1 clocks adds the clock time offset  $\tau_1$ . Similarly the time at receiver 2 can be written as

$$t_2 = t_0 + t_{02} + \tau_2 \quad (2.2)$$

with  $t_0$  as defined above,  $t_{02}$  is the pulse travel time to receiver 2 and  $\tau_2$  the clock offset time for receiver 2. Now if we take the case where both receivers are clock synchronized, then

$$\tau_1 = \tau_2$$

and taking the difference between the two receiver arrival times,

$$t_2 - t_1 = t_{01} - t_{02} = t_{\Delta} \quad (2.3)$$

where  $t_{\Delta}$  is the TDOA between the two receivers. Therefore, any time offset introduced by the asynchronous transmitter clock is eliminated by taking the time difference of arrival between two receivers that are clock synchronized. Transmitter design is simplified since synchronizing the clocks would require every transmitter to become a transceiver which would consume more power, increase its cost and its size. Since the mobile units are meant to be low cost, easily worn devices with long operation time per charge, a premium was placed on avoiding the inclusion of receiver circuitry in this unit. In the following chapters we will examine the theoretical performance that can be obtained when using TDOA-based location estimation in the face of several signal and system degradations.

## Chapter 3

# RTOA Estimation Performance

An important part of an end-to-end performance prediction is RTOA estimation error. In this chapter a Matlab RTOA estimation simulator is described and RTOA performance results presented. The simulation results are compared to analytical RTOA performance predictions. Experimental results supporting the simulation and analytical performance predictions are given. Finally, the analytical performance equations are used to generate nomographs that relate energy, fractional bandwidth and sensor spacing, which allows for system design utilizing the given system constraints.

### 3.1 A Matlab Simulator

We implemented a Matlab simulator based on the system block diagram shown in Fig. 3.1. Our multi-carrier signal is created using a random phase for each carrier which is then passed through an IFFT to obtain the time-domain signal. Random phases are used for the carriers in order to reduce the peak instantaneous power of the signal. Assigning the same phase to each carrier would result in a high instantaneous power in a narrow pulse of energy which is difficult to achieve in hardware. Separately, the system noise is modeled as a Gaussian random variable with variance of  $P_n$ . Due to the linearity of the FFT both signal and noise are processed through the FFT separately and the results added together before the SSE stage, which due to its non-linearity must process the noise and signal together. Finally, the noisy received data, along with a calibration phase vector, are processed by the

SSE which generates the RTOA estimate. The calibration phase vector is used to eliminate all the phase offsets added by system hardware. To obtain the calibration phase vector in our prototype system the phase data is captured and stored at each receiver once with the transmitter in a known location, then that phase data is used to phase correct all subsequent received data. One test signal is used for the specified number of Monte Carlo [6] trials along with the calibration phase vector created during the first trial. The rest of the simulation process is then repeated for the desired number of Monte Carlo tests with the intermediary and final results saved for analysis after all simulations are finished. Once all simulations are finished, system statistics can be calculated.

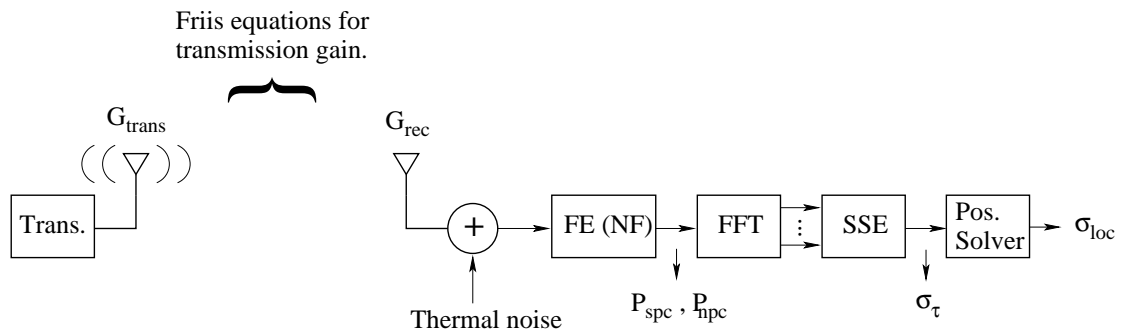


Figure 3.1: Matlab RTOA performance simulator block diagram.

## 3.2 Simulation Parameters

Parameters for characterizing the signal and system are specified by the user and summarized in Table 3.1. There are  $N$  samples in the discrete-time structure of the continuously transmitted waveform (Fig. 3.2) and the received signal hence  $N$  orthogonal frequency channels associated with this signal. The transmitted signal is made up of  $M$  carriers occupying a bandwidth,  $B$ , with the first carrier at index  $Fb$  in the length  $N$  signal channel vector. The distance between the transmitter and receiver antenna is  $R_{sep}$ , with an antenna temperature,  $T_{ant}$  and a transmitted power of  $P_{trans}$ .

These (Table 3.1) physical parameters are then used to derive the corresponding natural signal and system parameters used in the simulation. Using the Friis equation [7] the

$N$	Number of samples transmitted and received at a time
$M$	Number of carriers
$B$	Bandwidth
$Fb$	Index of first carrier in the signal
$R_{\text{sep}}$	Distance between transmitter & receiver antennas
$NF$	Noise figure
$T_{\text{ant}}$	Antenna noise temperature
$P_{\text{trans}}$	Transmitted power

Table 3.1: Specified system variables used in Matlab RTOA performance simulations.

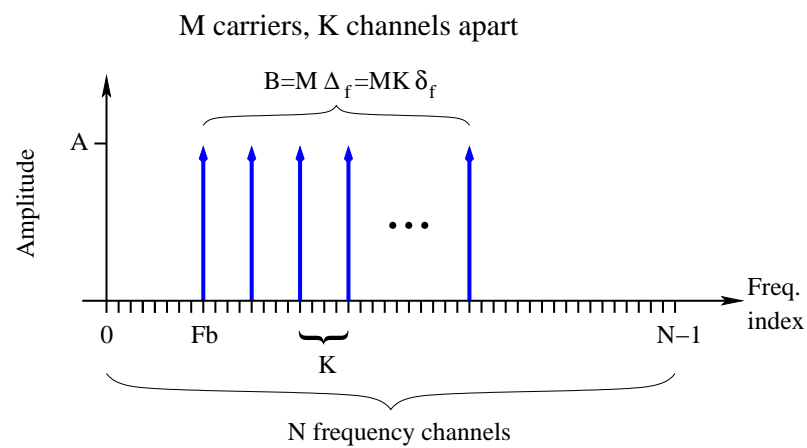


Figure 3.2: The multi-carrier signal

received signal power,  $P_s$  can be calculated.

$$P_s = \frac{P_{\text{trans}} G_{\text{trans}} G_{\text{rec}} \lambda^2}{16\pi^2 R_{\text{sep}}^2} \quad (3.1)$$

For this system both the transmitter antenna gain,  $G_{\text{trans}}$  and receiver antenna gain,  $G_{\text{rec}}$  are set to unity for omni-directional antennas. The RF signal wavelength,  $\lambda$  can be calculated from the bandwidth and the speed of light.

$$\lambda = \frac{c}{B}$$

By letting

$$G_0 = \frac{G_{\text{trans}} G_{\text{rec}} \lambda^2}{16\pi^2 R_{\text{sep}}^2},$$

the Friis equation (Eq. 3.1) can be rewritten as

$$P_s = P_{\text{trans}} G_0,$$

where  $G_0$  is referred to as the channel gain. In this simulator the  $M$  carriers are evenly spaced throughout the chosen bandwidth,  $B$  yielding a carrier spacing of  $K$ .

$$K = \frac{B}{M}$$

In order to satisfy the Nyquist rate the sampling rate,  $F_s$  is set to twice the bandwidth.

$$F_s = 2B$$

The noise power spectral density of the received signal is calculated from the specified antenna temperature,  $T_{\text{ant}}$  and noise figure,  $NF$ .

$$N_o = 4kT_{\text{ant}}10^{NF/10}$$

Next, the receiver side noise,  $P_n$  is based on the signal bandwidth,  $B$  and the noise power spectral density,  $N_o$ .

$$P_n = BN_o \quad (3.2)$$

Finally for these simulations the signal time duration,  $T$ , is related to the total number of samples in the signal,  $N$  and the bandwidth,  $B$  by

$$T = \frac{N}{2B}$$

Table 3.2 provides a summary of the derived parameters.

$K$	Carrier spacing
$P_s$	Received power
$\lambda$	wavelength
$G_o$	Channel gain factor
$T$	Time duration of signal
$N_o$	Noise Power Spectral Density
$F_s$	Sampling frequency
$P_n$	Noise power

Table 3.2: Calculated system variables used in Matlab RTOA performance simulations.

### 3.3 Calculating Simulation Statistics

The simulator calculates and saves signal statistics for each Monte Carlo test to form a data set for the specified number of Monte Carlo tests. The resulting data set is then used to form a performance analysis of the simulation results. Using the received power,  $P_s$  (calculated using Eq. 3.1), the multicarrier signal is constructed so that it has the specified power. Similarly the additive noise is formed using the calculated (Eq. 3.2) received noise power,  $P_n$  which is equivalent to the noise variance. In order to confirm that the signal and noise has the desired power, the sample variance of both is calculated. Eq. 3.3 shows the sample variance for both the received signal and noise, which is equivalent to the received signal power and noise at the FFT stage input.

$$P_s = \sigma_s^2 = \frac{1}{N} \sum_{k=1}^{N-1} s_k^2 \quad (3.3)$$

$$P_n = \sigma_n^2 = \frac{1}{N} \sum_{k=1}^{N-1} n_k^2$$

At the FFT stage output the signal and noise carrier data ( $M$  samples) is extracted from the received data ( $N$  samples) and saved from each Monte Carlo test for analysis after all tests are completed. Similarly, the RTOA estimate from the SSE stage output is also collected from each test.

Once all Monte Carlo tests are finished the performance statistics can be calculated. The received signal and noise power values,  $P_s$  and  $P_n$  (at the FFT input), that were calculated for each test are now averaged together and their corresponding SNR was calculated. The

signal and noise variances,  $\sigma_s^2$  and  $\sigma_n^2$  respectively, are calculated from the signal and noise data ( $M$  carriers only) captured at the FFT stage output and the corresponding per carrier SNR computed. Since the carrier SNR is the same across all  $M$  carriers, the mean carrier SNR is used. A RTOA estimate, from the SSE output, for each test is used to obtain the sample RTOA variance,  $\sigma_\tau^2$ .

### 3.4 Analytic Performance Prediction

In order to better understand the simulator's performance, it is useful to examine the expected performance limits on the RTOA estimate variance. Bhaskar Rao and K.S. Arun [2] presented an equation for the Cramer Rao Bound (CRB) of the variance.

$$E\{\Delta\Theta_k^2\}(CRB) = \left(\frac{6}{N^3}\right) \left(\frac{\sigma_n^2}{|c_1|^2}\right) \quad (3.4)$$

Here  $\Delta\Theta_k^2$  is the phase difference between carriers,  $\sigma_n^2$  is the noise variance and  $c_1$  the carrier amplitude. According to David Cyganski et al. [3], Eq. 3.4 can be rewritten using our system variables as the RTOA variance at SSE stage output.

$$\sigma_\tau^2(CRB) = \frac{3NP_n}{\pi^2 K^2 f_s^2 M^2 P_s} \quad (3.5)$$

Also, Rao and Arun provided [2] an expression for the variance of the phase difference for the SSE under optimum matrix shape conditions, which comes close to the CRB.

$$E\{\Delta\Theta_k^2\}(opt) = \left(\frac{27}{4N^3}\right) \left(\frac{\sigma_n^2}{|c_1|^2}\right) \quad (3.6)$$

We can express Eq. 3.6 in terms of our system variables.

$$\sigma_\tau^2(opt) = \frac{27NP_n}{8\pi^2 K^2 f_s^2 M^2 P_s} \quad (3.7)$$

Also an analytic expression for the SNR at the FFT stage output provides a way to confirm an intermediate simulation result.

$$SNR(FFTout) = \frac{NP_s}{2MP_n} \quad (3.8)$$

Eqs. 3.8, 3.7 and 3.5 allow the simulator output at the FFT and SSE stages to be confirmed.

### 3.5 Performance Simulations

For the simulations, a signal DFT vector length of  $N = 8192$  samples was used. A total of  $M = 132$  carriers, spaced  $K = 10$  channels apart, occupied a bandwidth of  $B = 7.1$  kHz between 2.153 kHz and 9.205 kHz. Transmitted signal power was set to 25.25 watts. Front-end noise figure was assumed to be 3 dB which corresponds to a noise figure factor of two. Omni-directional transmitter and receiver antennas, set 100 m apart were assumed along with an antenna noise temperature of  $290^\circ$  K. The wavelength of the RF signal,  $\lambda$ , was calculated using an RF frequency of 440 MHz. Table 3.3 summarizes the parameters used for these simulations. The parameters selected for these tests were chosen to facilitate our shakedown tests and are not representative of any practical system.

$N$	8192	Number of samples transmitted and received at a time
$M$	132	Number of carriers
$K$	10	Carrier spacing
$Fb$	400	Index of first carrier in the signal
$f_s$	44100 Hz	Sampling frequency
$B$	7.1 kHz	Bandwidth
$R_{\text{sep}}$	100 m	Distance between transmitter & receiver antennas
$NF$	3 dB	Noise figure
$T_{\text{ant}}$	$290^\circ$ K	Antenna temperature
$\lambda$	0.68135 in	RF signal wavelength
$P_{\text{trans}}$	25.25 W	Transmitted power
$G_o$	1	Channel gain factor
$P_s$	25.25 W	Received power
$P_n$	100 W	Noise power

Table 3.3: Specified signal parameters used in Matlab RTOA performance simulations.

A total of 500 Monte Carlo trials were performed using the simulation configuration in Table 3.3. Calculated SNR at the FFT stage output in the simulator was 8.936 dB which almost exactly matches the predicted result (using Eq. 3.8) of 8.942 dB. The FFT stage simulation and analytic performance results are summarized in Table 3.4. The simulation result for RTOA variance,  $\sigma_\tau^2(\text{sim})$  was  $3.2132\text{E} - 12 \text{ sec}^2$ . This result is close to the analytic RTOA variance,  $\sigma_\tau^2(\text{analytic})$  result of  $3.2731\text{E} - 12 \text{ sec}^2$  while both are bounded by the CRB RTOA variance,  $\sigma_\tau^2(\text{CRB})$  as expected. Table 3.5 summarizes the SSE stage

performance results. The remarkable agreement of the simulation and analytic results can be taken as confirmation of both our analytic model and the implementation of the end-to-end simulator. While only a single result is given here, these tools are used throughout this thesis to develop analytic performance design aids and will continue to be used to confirm experimental designs and results.

Stage Output	SNR [dB] (sim)	SNR [dB] (analytic)
FFT	8.936	8.942

Table 3.4: FFT stage simulation and analytic results.

Stage Output	$\sigma_\tau^2$ [sec] <sup>2</sup> (sim)	$\sigma_\tau^2$ [sec] <sup>2</sup> (analytic)	$\sigma_\tau^2$ [sec] <sup>2</sup> (CRB)
SSE	3.2132E-12	3.2731E-12	2.9094E-12

Table 3.5: SSE stage simulation and analytic results.

### 3.6 Nomographs

Nomographs are simple design aids and means to supply visual perspective on overall characteristics of the system [4]. For our location system, we wanted to examine the relationship between receiver geometry, signal bandwidth and energy. Fig. 3.3 shows a general geometry with some randomly placed receivers and one transmitter that is located a distance,  $r_o$  from the center of the receiver mass. While the geometry shown is 2-D, the results are equally valid for any 3-D geometry as well. John Bard et al. [1] presented a location error equation for this general receiver geometry:

$$\sigma_{\text{loc}}(\text{BardApprox.}) = cr_o\sigma_{\tau\Delta}\sqrt{\text{Tr}\{(\mathbf{A}^T\mathbf{A})^{-1}\}}, \quad (3.9)$$

where  $\mathbf{A}$  is the receiver position matrix. This equation is only asymptotically correct for  $r_o >$  sensor array effective radius, however related work [8] shows that its accuracy is still sufficient inside the array to obtain useful information regarding expected performance. For

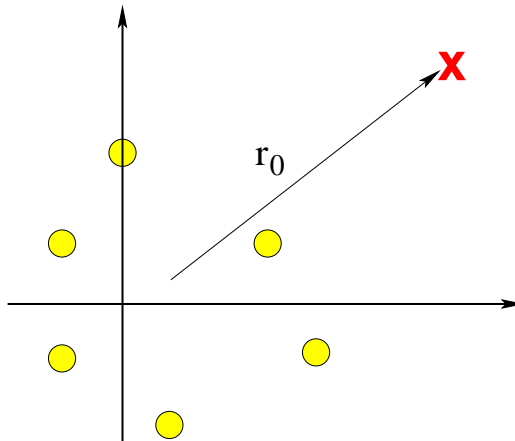


Figure 3.3: General receiver and transmitter geometry.

the purposes of generating a set of nomographs for a fixed single geometry of some general interest, the geometry of Fig. 3.3 was specified to consist of 3 receiver pairs located as shown in Fig. 3.4. Each receiver pair has one receiver in the x-y plane with the second transmitter located a distance  $h$  directly above. One receiver pair is placed at the origin with the others a distance  $w$  away along the x and y axis and the transmitter is placed some distance  $r_o$  from the receivers. Eq. 3.9 can now be written for this (Fig. 3.4) specific geometry.

$$\sigma_{\text{loc}} = \frac{1}{2} c r_o \sigma_{\tau \Delta} \sqrt{\frac{5}{w^2} + \frac{2}{h^2}} \quad (3.10)$$

Now we combine this special case (Eq. 3.10) with the CRB estimate for RTOA variance (Eq. 3.5) and the Friis equation (Eq. 3.1) to complete a location error equation for our specific geometry.

$$\sigma_{\text{loc}} = \frac{\sqrt{6} r_o \sqrt{k T_{\text{ant}} 10^{NF/10} E} \sqrt{5h^2 + 2w^2}}{EFh} \quad (3.11)$$

This location error equation (Eq. 3.11) can now be used to generate some system design aids. The nomograph in Fig. 3.5 relates fractional bandwidth, array length and energy for a location error of 1/10 m. Fractional bandwidth is defined as

$$F = \frac{B}{f_{\text{max}}}, \quad (3.12)$$

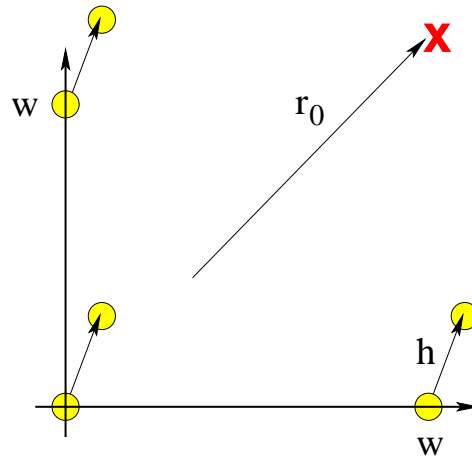


Figure 3.4: Specific receiver and transmitter geometry.

where  $f_{\max}$  is the maximum frequency in the signal. Array length is equivalent to  $w$  in Eq. 3.10. The series of contours represent system energy

$$E = P_{\text{trans}}T, \quad (3.13)$$

which combines transmitted power and transmitted signal period. The array length range for this nomograph, 5 – 30 m represents a reasonable receiver spacing for the application types envisioned for this locator. When our system is bandwidth limited, the fractional bandwidth is also reduced. This leads to a design decision to balance system energy and array size where energy may have to be increased in order to accommodate the array size requirement or if a smaller array size is acceptable then a lower energy requirement could be used. If bandwidth is not limited, it is a matter of determining an acceptable balance between energy and array size since increasing the bandwidth increases the energy flexibility. If energy is the constraining variable then the fractional bandwidth and array size will be constrained and system needs will have to be balanced. Observe that once system energy is above the 5E – 14 J both array length and fractional bandwidth choices are pretty flexible. Remember that this nomograph was generated for a particular geometry, number of RNs, ect. so if the system requirements don't result in a practical design, then changing some of these parameters may be propitious. The value of our development is that the general form it takes allows one to generate a suitable nomograph for any geometry (and other

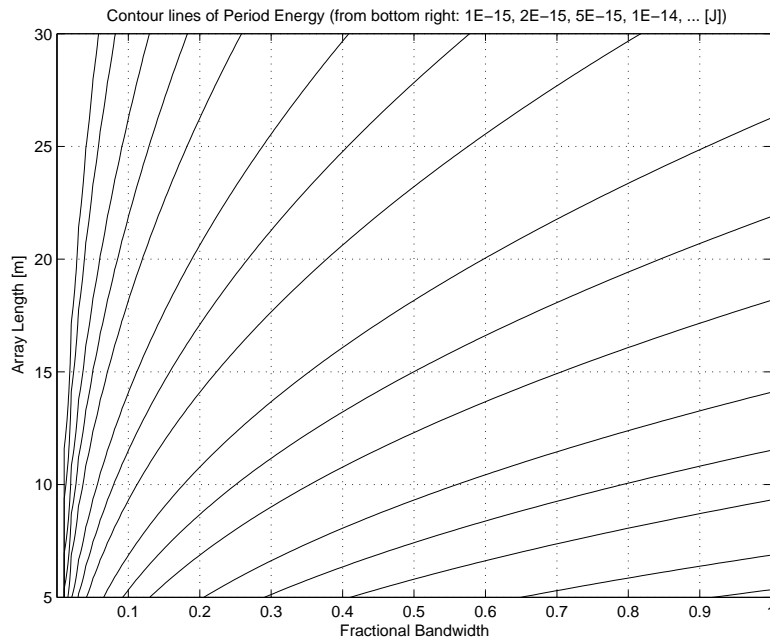


Figure 3.5: Energy, bandwidth and vector length nomograph.

variations) of interest.

Now let's work through a design example using the nomograph. If the following parameters are chosen, what is the required transmitted power to achieve a location accuracy of 1/10 m?

Array length, $w = 25$ m $f_{\max} = 1$ GHz Bandwidth, $B = 400$ MHz
--

The fractional bandwidth,  $F$ , is calculated from Eq. 3.12 using the  $f_{\max}$  and  $B$  values for this example.

$$F = \frac{400 \text{ MHz}}{1 \text{ GHz}} = 0.4$$

Next, if we have 1 M samples of storage and we sample at 400 M samples-per-sec, the period,  $T$  can be calculated.

$$T = \frac{1 \text{ M samples}}{400 \text{ M samples/sec}} = 0.0025 \text{ sec}$$

If we choose an energy,  $E$  of  $1\text{E-}12$  Joules then the necessary transmitted power is:

$$P_{\text{trans}} = \frac{E}{T} = 3\text{E-}10 \text{ watts}$$

Therefore, we can achieve our location accuracy goal of  $1/10$  m with a transmitted power of only  $0.3$  nW.

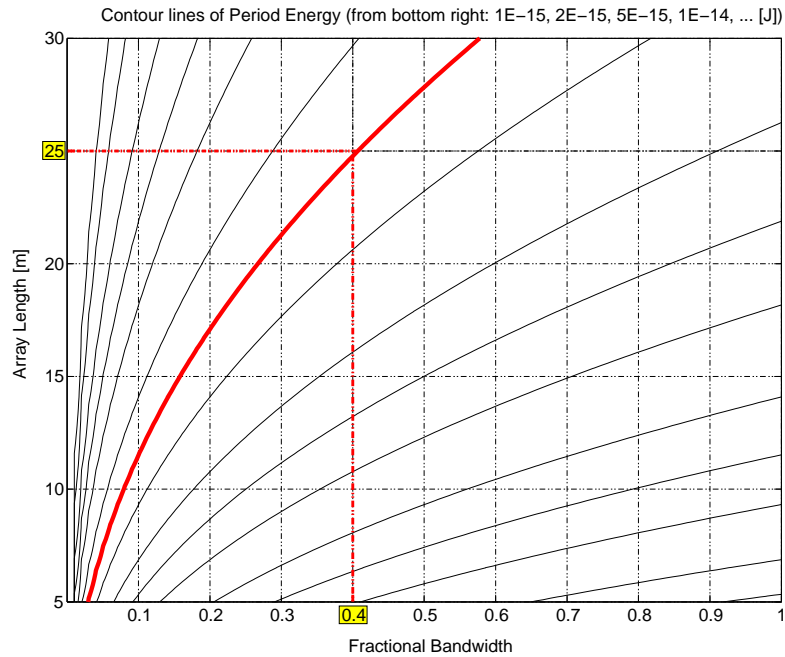


Figure 3.6: System design example nomograph.

### 3.7 Experimental Performance

While both the Matlab simulation results and the analytical prediction results agree, we now need to confirm the performance estimates using the demonstrator system described in Sec. 2.2. In order to extract the necessary information from the demonstrator, it was necessary to add the ability to calculate the relevant signal statistics. Fig. 3.7 is a block diagram of the demonstrator system showing each stage and the statistics that are extracted the stage outputs.

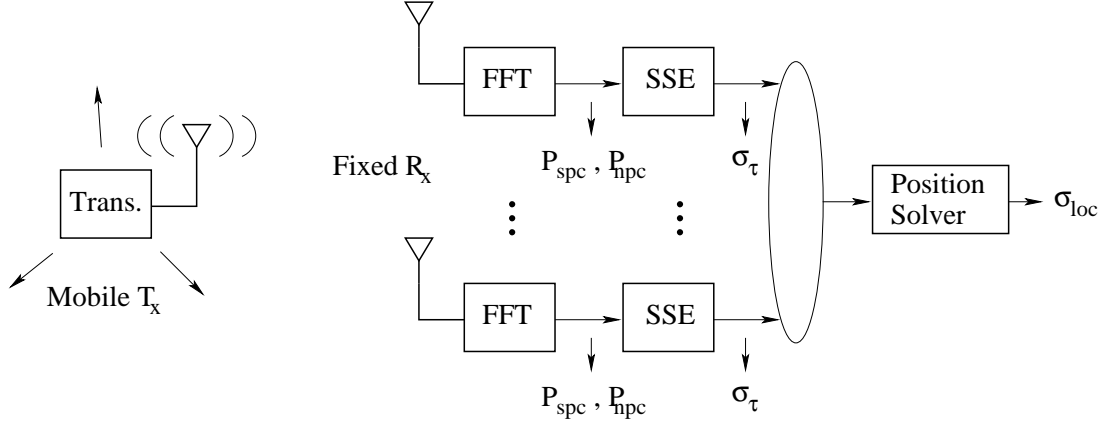


Figure 3.7: Instrumented audio demonstrator block diagram.

As before our signal consists of  $M$  carriers in an  $N$  sample signal. First we average each carrier amplitude over  $\beta_{\max}$  tests.

$$\bar{F}_\nu = \frac{1}{\beta_{\max}} \sum_{\beta=0}^{\beta_{\max}-1} F_{\nu,\beta},$$

where  $\nu$  indexes the  $M$  carriers in our signal. Using the carrier amplitude averages,  $\bar{F}_\nu$ , the signal-power-per-channel can now be formed.

$$P_{\text{spc}} = \bar{F}_G^2 = \frac{1}{M^2} \sum_{\nu=0}^{M-1} |\bar{F}_\nu|^2$$

Now we can calculate a standard deviation for each carrier.

$$\sigma_\nu^2 = \frac{1}{\beta_{\max} - 1} \sum_{\beta=0}^{\beta_{\max}-1} |F_{\nu,\beta} - \bar{F}_\nu|^2$$

The noise power-per-channel,  $P_{\text{npc}}$ , is calculated as follows.

$$P_{\text{npc}} = \sigma_G^2 = \frac{1}{M} \sum_{\nu=0}^{M-1} \sigma_\nu^2$$

The RTOA estimates for each cycle are accumulated and after all tests are finished the time estimate variance,  $\sigma_\tau^2$ , calculated.

$$\bar{\tau} = \frac{1}{\beta_{\max}} \sum_{\beta=0}^{\beta_{\max}-1} \tau_\beta$$

$$\sigma_{\tau}^2 = \frac{1}{\beta_{\max} - 1} \sum_{\beta=0}^{\beta_{\max}-1} (\tau_{\beta} - \bar{\tau})^2$$

Finally, the location estimate standard deviation,  $\sigma_{\text{loc}}^2$ , can be calculated.

$$\bar{\tau}_{\text{xyz}} = \frac{1}{\beta_{\max}} \sum_{\beta=0}^{\beta_{\max}-1} \tau_{\text{xyz},\beta}$$

$$\sigma_{\text{loc,xyz}}^2 = \frac{1}{\beta_{\max} - 1} \sum_{\beta=0}^{\beta_{\max}-1} (\tau_{\text{xyz},\beta} - \bar{\tau}_{\text{xyz}})^2$$

$$\sigma_{\text{loc}}^2 = \frac{1}{\beta_{\max}} \sum_{\beta=0}^{\beta_{\max}-1} \sigma_{\text{loc,xyz}}^2$$

In this experiment we transmitted our audio multi-carrier signal which consisted of  $N = 8192$  samples and  $M = 101$  carriers separated by  $K = 10$  samples. The results in

Signal Samples, $N = 8192$
Carriers, $M = 101$
Carrier Spacing, $K = 10$
Receivers = 4
Monte Carlo Tests = 1000

Table 3.6: Parameters used for experimental RTOA performance results in Table 3.7.

Table 3.7 show the performance statistics from four experiments, each consisting of 1000 Monte Carlo trials, alongside the analytical predictions. The RTOA variance,  $\sigma_{\tau}$  measured

SNR [dB]	$\sigma_{\tau}$ [sec] (meas.)	$\sigma_{\tau}^2$ [sec <sup>2</sup> ] (meas.)	$\sigma_{\tau}^2$ [sec <sup>2</sup> ] (pred.)	$\sigma_{\text{loc}}$ [in] (meas.)	$\sigma_{\text{loc}}$ [in] (pred.)
-12.1	1.46E-6	1.18E-12	5.04E-12	0.0423	0.0768
-10.1	1.81E-6	1.08E-12	4.02E-12	0.0573	0.1020
-11.8	1.49E-6	1.25E-12	4.89E-12	0.0527	0.0739
-14.0	1.56E-6	1.33E-12	6.28E-12	0.0523	0.0740

Table 3.7: Measured and predicted experimental performance results.

at the demonstrator's SSE stage output ranges from  $1.08\text{E} - 12$  to  $1.33\text{E} - 12 \text{ sec}^2$ . while the predicted RTOA variance has a range of  $4.02\text{E} - 12$  to  $6.28\text{E} - 12 \text{ sec}^2$ . Both experimental and analytical RTOA values are quite consistent and are equal in order of magnitude.

The analytically predicted RTOA value is consistently larger than the experimental result. Our experimental location error,  $\sigma_{loc}$  is small with a maximum error standard deviation of 0.0573 in. compared to a maximum analytically predicted location error standard deviation of 0.102 in. Again the experimental results are consistently better than the predicted results. The small difference between predicted and measured values is probably due to inaccuracy in the measurement of the SNR within the experimental context. These tests confirmed for us that our experimental system operation was correct and was not subject to any loss of performance to unidentified design flaws or unpredicted noise sources.

## Chapter 4

# Frequency Skew and Shift Effects

Since there are limits to the amount of RTOA error that the location algorithm can tolerate without exceeding the maximum location error, it is necessary to examine potential sources of RTOA error. A couple of important error sources are frequency skew and frequency shift. Since the transmitter clock isn't synchronized with the receiver's clocks a phase shift is introduced in our carrier phase estimates. As long as this phase shift is constant or changes linearly with frequency of the carriers, then our system can handle it. A Matlab simulator was written to help investigate the impact frequency skew and shift have on RTOA estimation in our system. The simulation's results were confirmed analytically using Maple and experimentally with the audio demonstrator.

When the transmitter and receiver clock's are perfectly matched, then the carriers are at the expected frequency as illustrated in Fig. 4.1. Frequency shift occurs when the local heterodyne oscillator frequency in the transmitter differs from the receiver's local heterodyne oscillator frequency by some value,  $\delta_\Omega$  that is the same for all carriers. This is shown in Fig. 4.2. Frequency skew results if the sampling frequency of the transmitter's clock and the receiver's clock are not exactly the same, but differ by some constant,  $\gamma$ . Here the received signal carriers exhibit a stretching effect where the  $n^{\text{th}}$  carrier is offset by  $n\epsilon$  as pictured in Fig. 4.3. While frequency skew can occur in both direct conversion and heterodyne receivers, frequency shift only happens in heterodyne receivers.

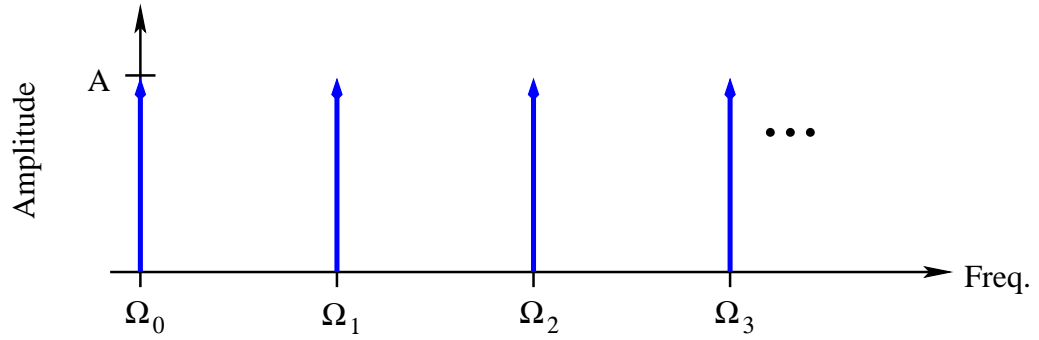


Figure 4.1: Clock synchronized: Amplitude  $A$  carriers are captured perfectly.

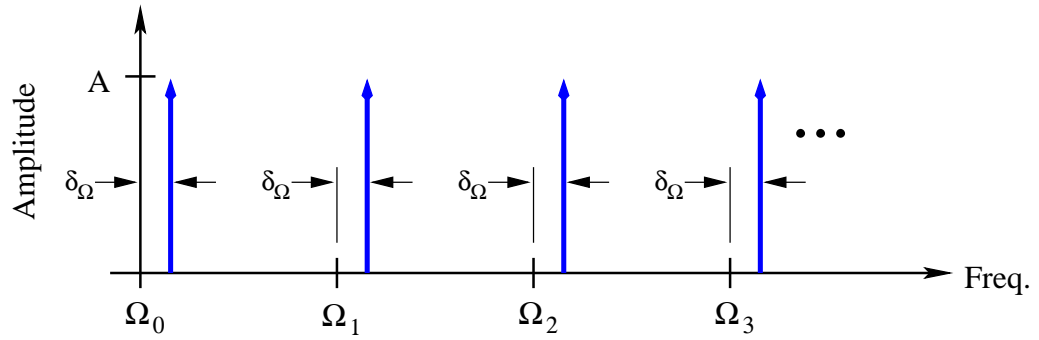


Figure 4.2: Frequency shift: Amplitude  $A$  carriers are offset a constant  $\delta_\Omega$ .

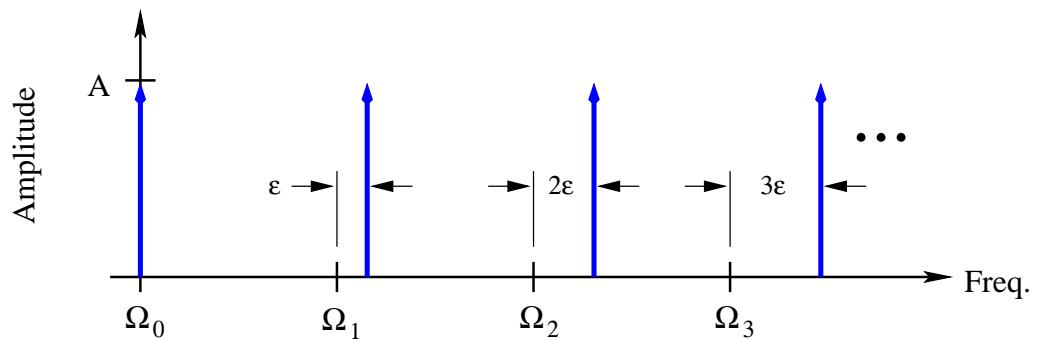


Figure 4.3: Frequency skew: Amplitude  $A$  carriers are offset by  $n\varepsilon$ .

## 4.1 Matlab Simulator

In order to determine the effect frequency skew and shift has on the RTOA estimation, a simulator was implemented in Matlab. Normally, the transmitted signal is constructed from specified frequency-domain components passed through an IFFT to obtain the samples of the associated time-domain signal. This construction method is efficient, but doesn't provide an easy method for adding frequency skew and shift effects to the signal. Instead, an alternate version of the signal generation function was written that builds the time-domain signal directly. This allows easy adjustment of any frequency skew and shift introduced into the signal.

The simulator uses our  $N$ -point discrete multi-carrier signal. Each of the  $M$  carriers are computed using a random phase,  $\phi_n$  as explained earlier. Eq. 4.1 is the discrete time-domain signal as it was constructed directly, without any provision for adding frequency skew or shift effects. This is equivalent to the signal built from specified frequency-domain components and passed through an IFFT.

$$s[m] = \sum_{n=0}^{M-1} \cos\left(\frac{2\pi(m-1)(Fb + nK)}{N} + \phi_n\right), m \in 1 \dots N \quad (4.1)$$

Alternatively, the signal can be constructed with the desired frequency skew and shift effects to simulate the actual hardware situation.

$$s[m] = \sum_{n=0}^{M-1} \cos\left(\frac{2\pi(m-1)(Fb + f_{\text{shift}} + nKf_{\text{skew}})}{N} + \phi_n\right), m \in 1 \dots N \quad (4.2)$$

Note that when  $f_{\text{skew}} = 1$  and  $f_{\text{shift}} = 0$  Eq. 4.2 reduces to Eq. 4.1. In our simulations we were interested in RTOA estimates for signals with  $f_{\text{skew}} \approx 1$  and  $f_{\text{shift}} \approx 0$ .

Our goal in this part of the work, as previously mentioned, is to construct a general purpose simulator which can be easily configured to emulate any given signal structure and non-ideal transmitter and receiver implementations. To make our exposition easy to follow, in the following we will use a specific set of values chosen only for simplicity of the description. Our test signal had 8192 samples with 101 carriers starting at the 400th sample and each separated by 10 channels. With a sampling rate of 8192 MHz, those parameters translate to a signal bandwidth of 1 GHz centered at 900 MHz. Simulation

$N$	8192	Number of samples transmitted and received at a time
$M$	101	Number of carriers
$K$	10	Carrier spacing
$Fb$	400	Index of first carrier in the signal
$F_s$	8192 MHz	Sampling frequency
$B$	1 GHz	Bandwidth

Table 4.1: Example freq. skew and shift Matlab simulation signal parameters used in the discussion of Sections 4.1 and 4.2.

starts with the construction of the signal with the chosen  $f_{\text{skew}}$  and  $f_{\text{shift}}$  parameters and some random phase for the carriers. After passing the signal through an FFT, the carrier data is calibrated by dividing by the complex phasors used to build the signal. In an actual system the calibration data would be created from the captured carrier data in order to eliminate phase shifts inherent in the system, but in this simulation that is not necessary. Once the carrier data is calibrated, it is ready for the SSE which estimates the RTOA for this trial. The RTOA estimation for each trial is stored and when all trial are completed, the results plotted so that the RTOA behavior can be observed. For frequency skew we plotted RTOA time offset as a function of the ratio of the transmitter and receiver sampling clock frequencies over a frequency skew factor range. Frequency shift is plotted as a function of local oscillator shift in terms of a fraction of the carrier spacing for an oscillator shift channel fraction range.

## 4.2 Simulation Results

Once the simulator was working, the first step was to test its operation using a frequency skew range reflective of actual crystal oscillator tolerances. ICM (International Crystal Manufacturing Co, Inc) gives a tolerance of  $\pm 10$  ppm for precision crystals [5]. This tolerance translates into a frequency skew factor range of  $1 \pm 0.00001$ . Running the simulator with that  $f_{\text{skew}}$  range yielded a RTOA range of  $\pm 5$  ps (Fig. 4.4), which is well within the maximum TDOA permissible error range of 200 ps [8]. This indicates that for practical crystal oscillator tolerances frequency skew will affect RTOA estimation, but not enough for the system to fail. Now we can fix frequency skew at 0.00001 and sweep fre-

quency shift for  $\pm 0.5$ . The peak RTOA for this test (Fig. 4.5) is 4 ps which again is well below our maximum allowed value.

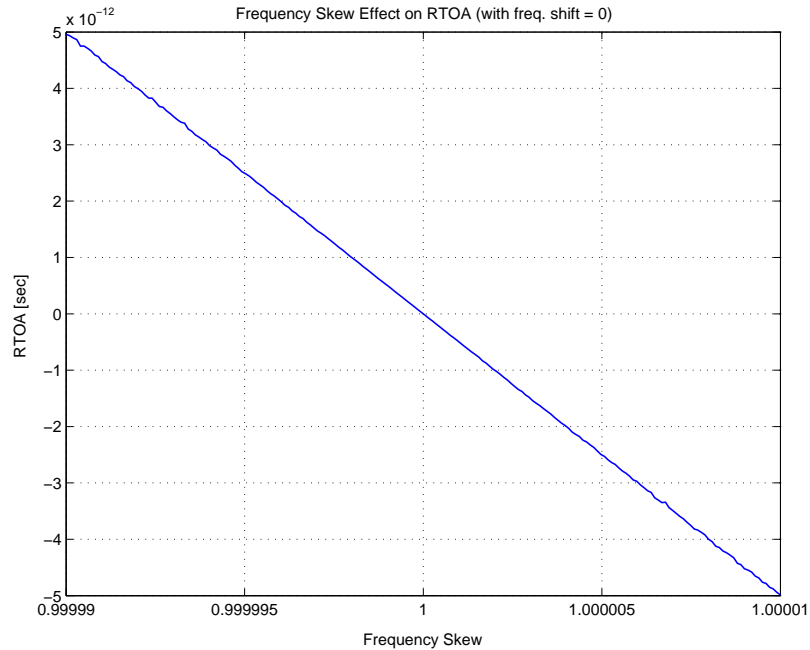


Figure 4.4: RTOA estimate with  $\pm 0.00001$  freq. skew factor.

Now we know that the system can tolerate at least some frequency skew, we need to determine the range within which frequency skew has an effect on RTOA estimation sufficiently small and well behaved as to allow an expectation of cancellation after TDOA formation. The skew effect can be tolerated as long as the amount is small enough such that the resulting TDOAs are perturbed by less than 200 ps. Using the  $f_{\text{skew}} = 1 \pm 0.00001$  range as a starting point, more skew was added until the RTOA estimate sufficiently broke down. A RTOA estimate was obtained for 200 evenly spaced points within the frequency range. A skew range of  $1 \pm 0.0112$  (Fig. 4.6) shows that the RTOA response is linear for most of this range and becomes non-linear near the endpoints. Given the cancellation of small consistent error by TDOA processing, we expect unperturbed location estimation at least throughout this linear range.

Similarly, the impact of frequency shift was explored to determine the effect on RTOA

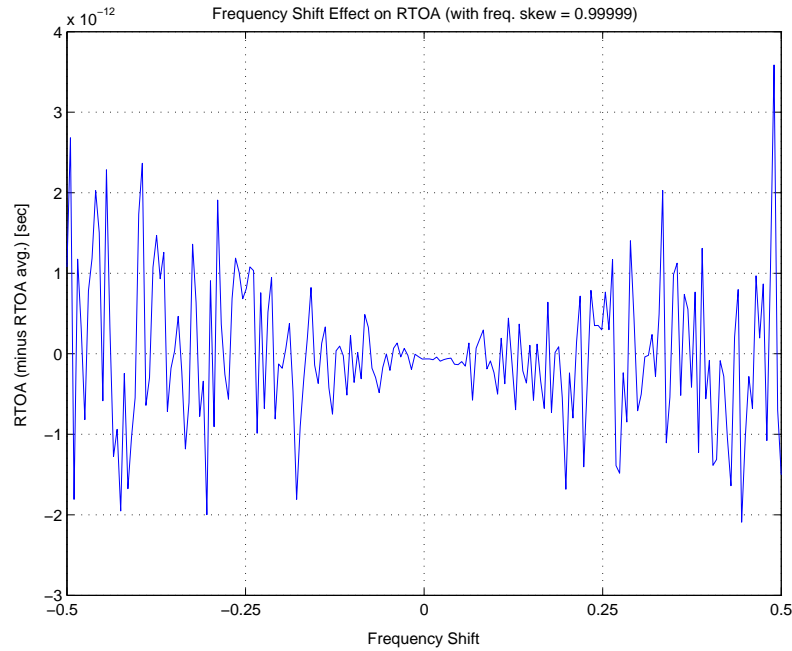


Figure 4.5: RTOA estimate with 0.00001 freq. skew factor and  $\pm 0.5$  oscillator shift channel fraction.

estimation. Since all the receivers are clock synchronized, the phase shift caused by sufficiently small frequency shift should be consistent between all receivers. Therefore, since we are using TDOAs, that phase shift should subtract out when calculating the TDOA between two receiver's. The initial trial of  $\pm 0.5$  shift showed that the RTOA estimation was about  $\pm 9$  ps, which is well within our TDOA limit of 200 ps. When frequency shift was increased to  $\pm 6.1$ , the RTOA estimate now approached the 200 ps limit (Fig. 4.7). Clearly by itself a large amount of frequency skew can be tolerated.

Now, we can zoom in and focus on the region (Fig. 4.6) where in the RTOA estimation response is linear. After decreasing the skew and re-running the test, it was found that a skew range of  $1 \pm 0.01008$  seemed to capture most of the linear RTOA estimate range (Fig. 4.8). A linear line was fit to this data since we are interested in how much the data varies from that line. By subtracting the linearly fit line from our data, we can examine how much the RTOA estimation varies from the line. As long as the deviation is less than 200 ps, the locator should work within our desired performance specifications [8]. Fig. 4.8 shows that

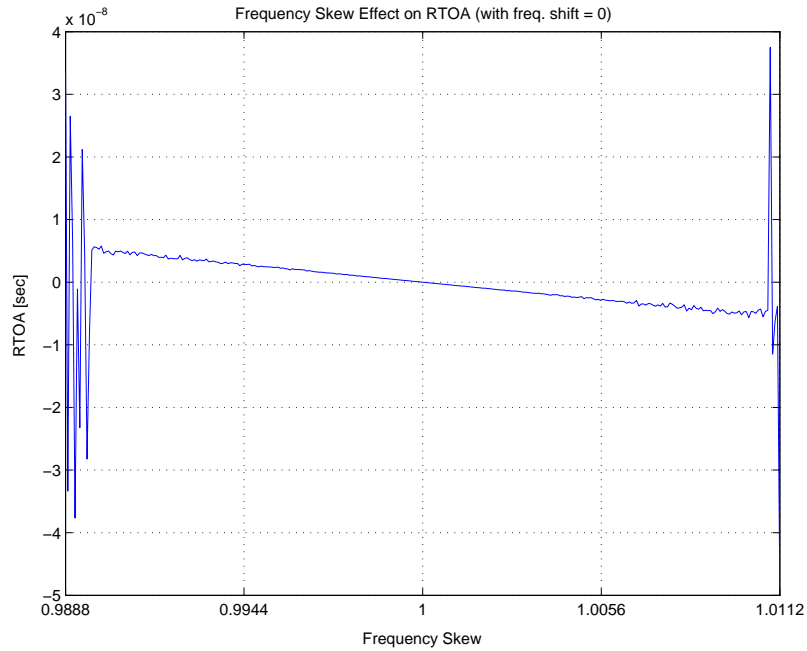


Figure 4.6: RTOA offset as a function of the ratio of  $T_x$  and RN clock frequencies (freq. skew factor).

only near the endpoints of the graph does the RTOA estimate approach and exceed our 200 ps threshold.

With the endpoints of the linear RTOA response region established it is worthwhile looking at the effect frequency shift has at those frequency skew values. Using fixed  $f_{skew}$  values of 0.98992 and 1.01008,  $f_{shift}$  was swept in a range of  $\pm 0.1$ . Fig. 4.10 and Fig. 4.11 show that the RTOA estimate only exceeds the 200 ps when the frequency shift exceeds 0.05. Reducing the frequency skew range to  $\pm 0.00952$  places the RTOA estimation a little further away from the non-linear response region of Fig. 4.6. The frequency shift is again swept in the  $\pm 0.1$  range. Now the RTOA estimation stays below the threshold for the entire shift range.

All these simulations were performed for a signal with specific frequency characteristics as described above. In order to examine how well these results scale when the bandwidth is reduced to 10 kHz and the carriers are 100 Hz apart, we conducted some of the same tests for the limited bandwidth case. A frequency skew range of  $1 \pm 0.01008$  produces a linear

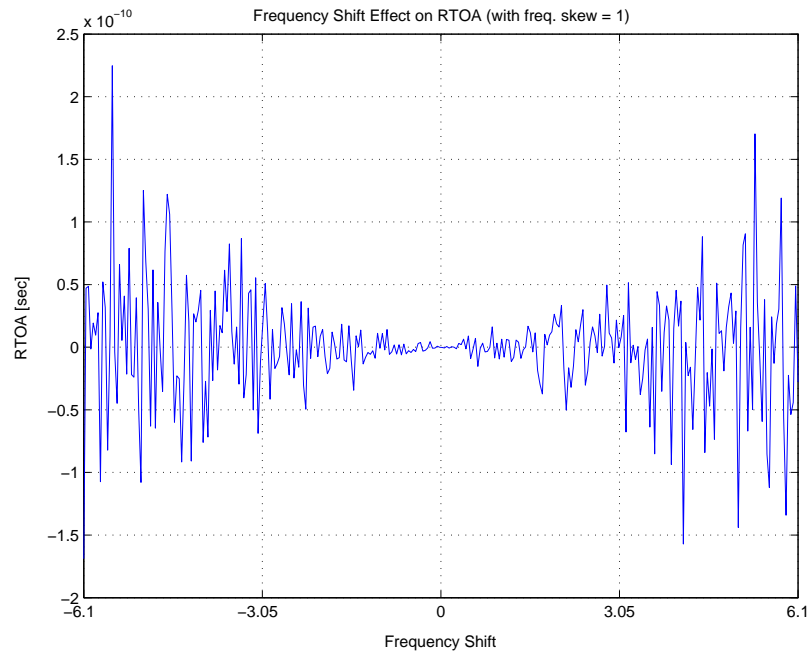


Figure 4.7: RTOA offset as a function of local oscillator shift in terms of a fraction of the carrier spacing (oscillator shift channel fraction).

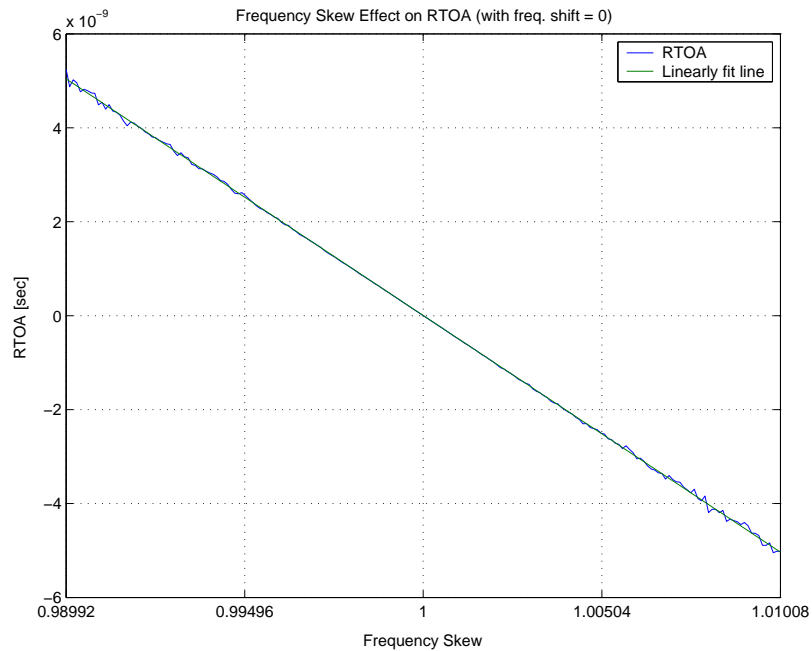


Figure 4.8: RTOA estimate with  $\pm 0.01008$  freq. skew factor.

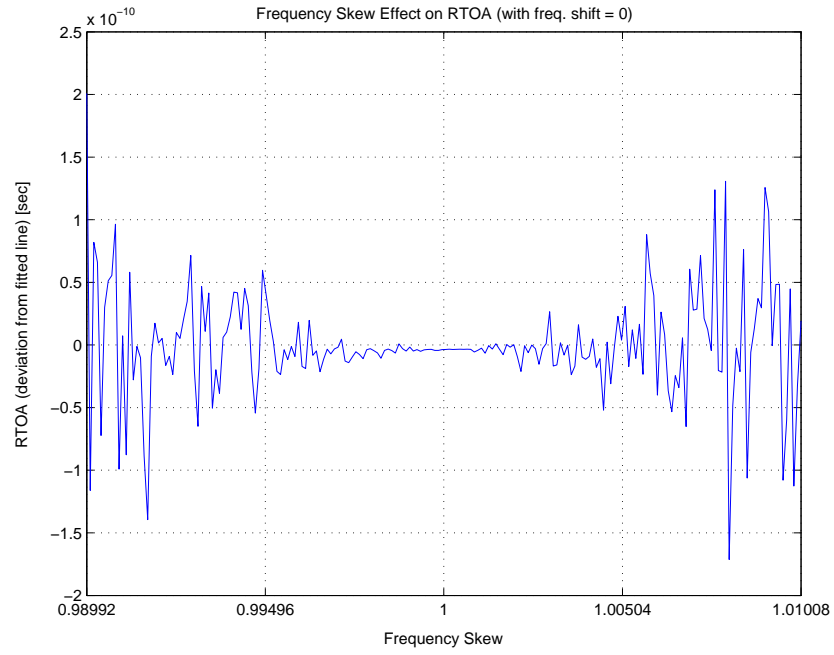


Figure 4.9: RTOA estimate deviation with  $\pm 0.01008$  freq. skew factor.

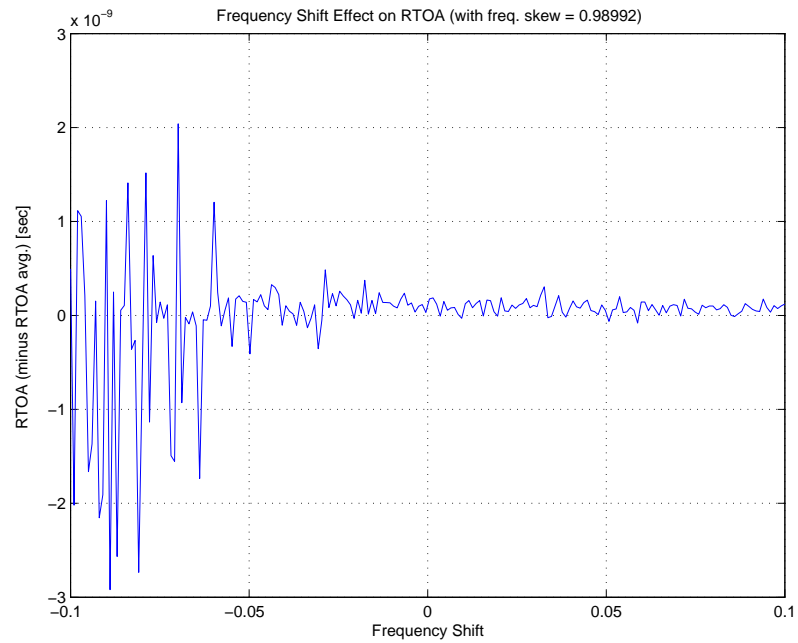


Figure 4.10: RTOA estimate with 0.98992 freq. skew factor and  $\pm 0.1$  oscillator shift channel fraction.

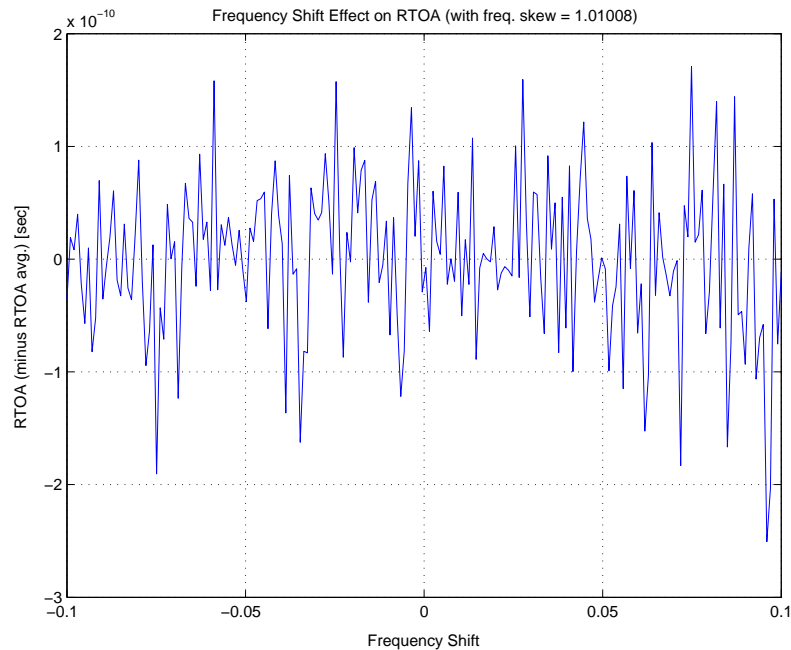


Figure 4.11: RTOA estimate with 0.01008 freq. skew factor and  $\pm 0.1$  oscillator shift channel fraction.

TOA (Fig. 4.14) response similar to Fig. 4.8. However, examining the TOA deviation from a linearly fit line (Fig. 4.15) shows a TOA variation of  $\pm 50 \mu\text{s}$  which is nowhere near our threshold of 200 ps. As bandwidth is reduced and the carriers get closer in frequency, TOA estimation is affected more severely by frequency skew. Similarly, frequency shift has more of an impact on TOA performance for this case. Fig. 4.16 is the TOA performance for a frequency shift range of  $\pm 0.5$ . The TOA range is  $\pm 1000 \text{ ns}$  which is again far short of our 200 ps threshold.

While the simulator we have constructed is useful for confirming specific implementation behaviors better means are needed to establish general behavior such as the scaling of parameter deviation bounds such as those briefly explored above. For these purposes an analytic estimate of RTOA deviation is most appropriate. We develop such a result in the next section.

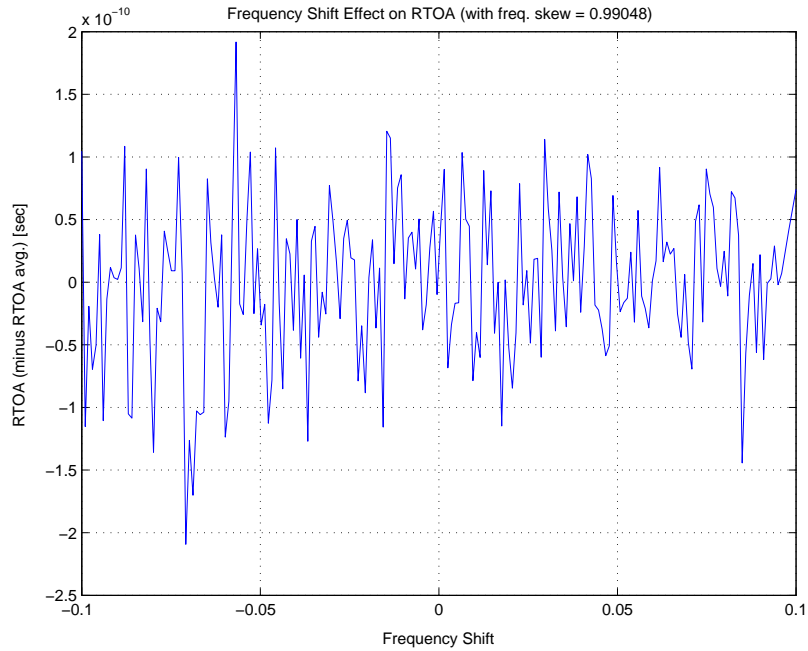


Figure 4.12: RTOA estimate with 0.99048 freq. skew factor and  $\pm 0.1$  oscillator shift channel fraction.

### 4.3 Analytical Results

The ideal case occurs when there are no frequency skew and shift effects. Our multi-carrier signal can be written as a sum of complex exponentials.

$$s(m) = \frac{1}{N} \sum_{n=0}^{N-1} A_n e^{j\Omega_n m} \quad (4.3)$$

We are interested in the DFT of our signal (Eq. 4.3).

$$S(k) = \frac{1}{N} \sum_{m=0}^{N-1} \sum_{n=0}^{N-1} A_n e^{j\Omega_n m} e^{-j\Omega_k m} \quad (4.4)$$

Both  $\Omega_n$  and  $\Omega_k$  in Eq. 4.10, can be rewritten as

$$\Omega_n = \frac{2\pi n}{N}, \quad \Omega_k = \frac{2\pi k}{N} \quad (4.5)$$

and substituting into Eq. 4.4 gives:

$$S(k) = \frac{1}{N} \sum_{m=0}^{N-1} \sum_{n=0}^{N-1} A_n e^{\frac{j2\pi nm}{N}} e^{-\frac{j2\pi km}{N}} \quad (4.6)$$

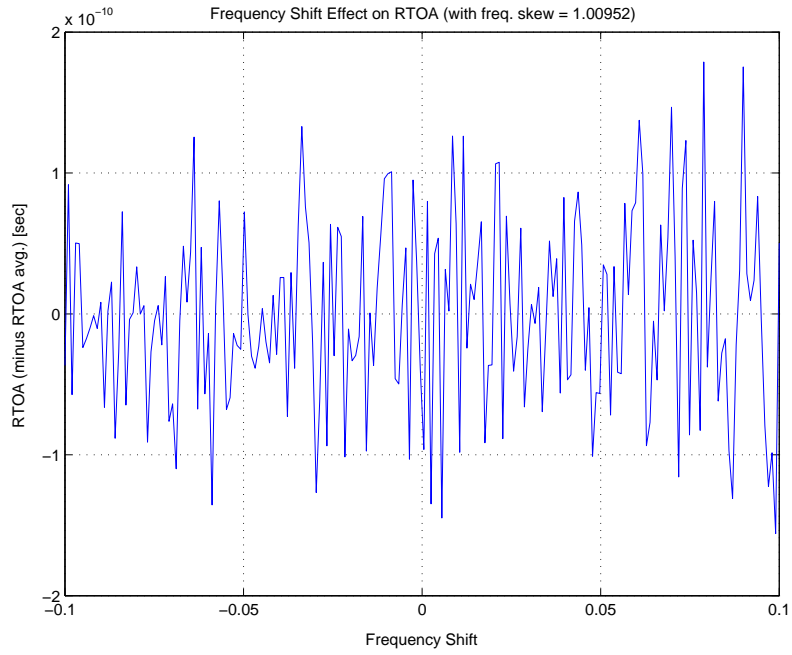


Figure 4.13: RTOA estimate with 0.00952 freq. skew factor and  $\pm 0.1$  oscillator shift channel fraction.

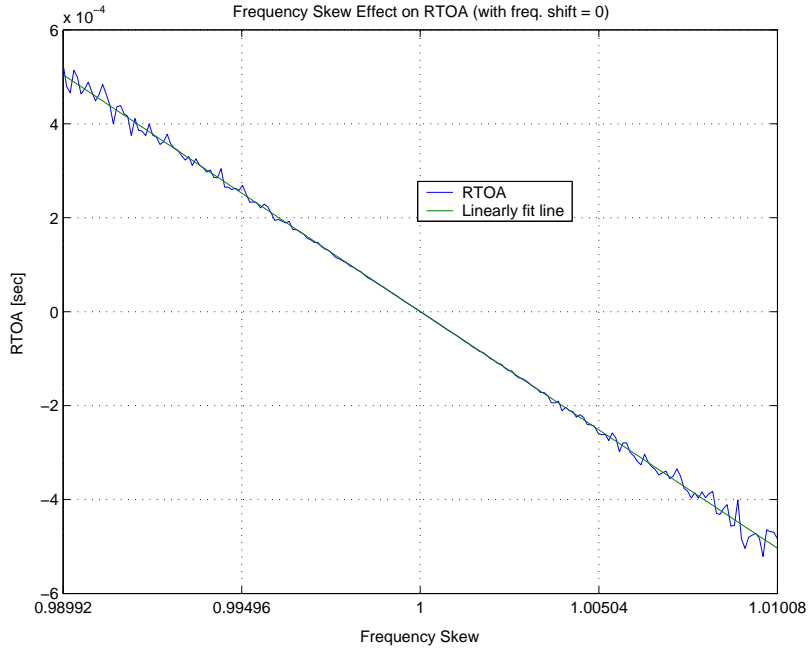


Figure 4.14: RTOA estimate with  $\pm 0.01008$  freq. skew factor.

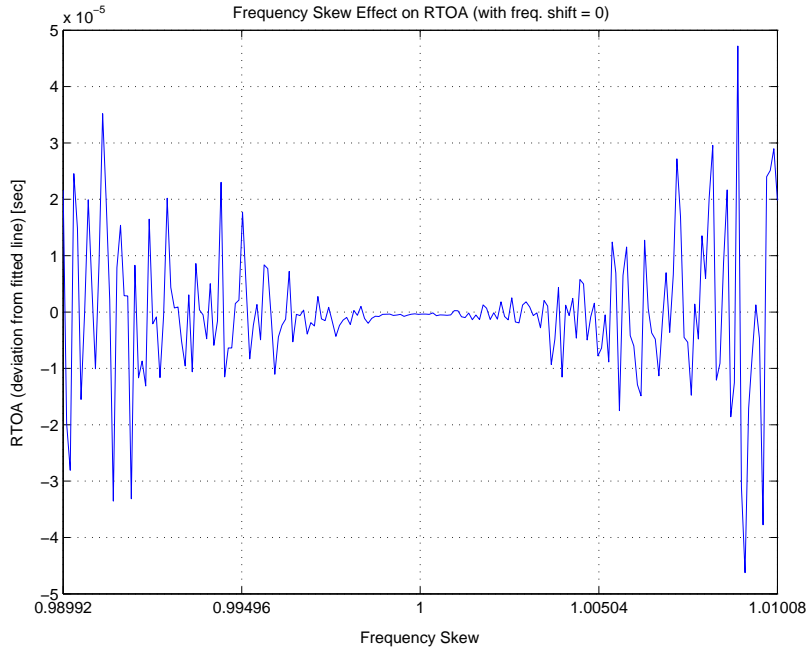


Figure 4.15: RTOA estimate deviation with  $\pm 0.01008$  freq. skew factor.

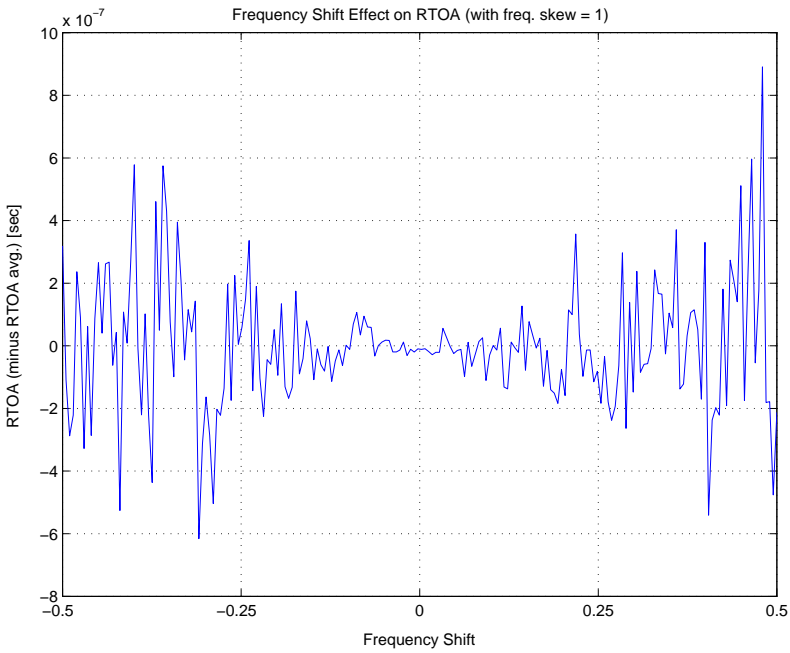


Figure 4.16: RTOA estimate with  $\pm 0.5$  oscillator shift channel fraction.

Eq. 4.6 can be simplified and the order of the summations reversed.

$$S(k) = \frac{1}{N} \sum_{n=0}^{N-1} A_n \sum_{m=0}^{N-1} e^{\frac{j2\pi(n-k)m}{N}} \quad (4.7)$$

The inner summation is non-zero only when  $n = k$ , therefore the closed form solution for the inner sum is known and Eq. 4.7 can be evaluated.

$$S(k) = \frac{1}{N} A_k N = A_k \quad (4.8)$$

The result is the solution for our ideal case.

In the non-ideal case we have frequency skew and shift effects on phase and Eq. 4.3 can be rewritten as

$$\tilde{s}(m) = \frac{1}{N} \sum_{n=0}^{N-1} A_n e^{j(\gamma\Omega_n + \delta_\Omega)m}, \quad (4.9)$$

where  $\gamma$  is the frequency skew and  $\delta_\Omega$  the frequency shift. Now we can take the DFT of Eq. 4.9:

$$\tilde{S}(k) = \frac{1}{N} \sum_{m=0}^{N-1} \sum_{n=0}^{N-1} A_n e^{j(\gamma\Omega_n + \delta_\Omega)m} e^{-j\Omega_k m} \quad (4.10)$$

Substituting the frequency relationships of Eq. 4.5 and letting  $\gamma = 1 + \epsilon$ , which allows for evaluating frequency skew for values of  $\epsilon \approx 0$ , we obtain.

$$\tilde{S}(k) = \frac{1}{N} \sum_{m=0}^{N-1} \sum_{n=0}^{N-1} A_n e^{j\left(\frac{2\pi\gamma n}{N} + \delta_\Omega\right)m} e^{-\frac{j2\pi km}{N}} \quad (4.11)$$

$$\tilde{S}(k) = \frac{1}{N} \sum_{m=0}^{N-1} \sum_{n=0}^{N-1} A_n e^{j\left(\frac{2(1+\epsilon)\pi n}{N} + \delta_\Omega\right)m} e^{-\frac{j2\pi km}{N}} \quad (4.12)$$

Taking the Taylor expansion of Eq. 4.12 about  $\epsilon = 0$  and  $\delta_\Omega = 0$ :

$$\begin{aligned} \tilde{S}(k) &= \frac{1}{N} \sum_{m=0}^{N-1} \sum_{n=0}^{N-1} A_n e^{\frac{j2\pi nm}{N}} e^{-\frac{j2\pi km}{N}} \\ &+ \frac{1}{N} \sum_{m=0}^{N-1} \sum_{n=0}^{N-1} j A_n e^{\frac{j2\pi nm}{N}} \left( \frac{2\epsilon\pi n}{N} + \delta_\Omega \right) m e^{-\frac{j2\pi km}{N}} \\ &+ \frac{1}{N} \sum_{m=0}^{N-1} \sum_{n=0}^{N-1} -\frac{1}{2} A_n e^{\frac{j2\pi nm}{N}} \left( \frac{2\pi\epsilon n}{N} + \delta_\Omega \right)^2 m^2 e^{-\frac{j2\pi km}{N}} \\ &+ \frac{1}{N} \sum_{m=0}^{N-1} \sum_{n=0}^{N-1} -\frac{1}{6} j A_n e^{\frac{j2\pi nm}{N}} \left( \frac{2\pi\epsilon n}{N} + \delta_\Omega \right)^3 m^3 e^{-\frac{j2\pi km}{N}} \end{aligned} \quad (4.13)$$

Note that in the case where there is no frequency skew and shift, i.e.

$$\epsilon = 0 \text{ and } \delta_\Omega = 0$$

the Taylor expansion reduces to

$$\tilde{S}(k) = \frac{1}{N} \sum_{m=0}^{N-1} \sum_{n=0}^{N-1} A_n e^{\frac{j2\pi nm}{N}} e^{-\frac{j2\pi km}{N}}$$

which is the ideal case in Eq. 4.6. We are interested in the last three terms of the Taylor expansion since they are responsible for all the non-ideal effects. Also, the amplitude,  $A_n$ , is set to unity since this simplification reflects our actual transmitted signal.

$$\begin{aligned} \tilde{S}(k) &= \frac{1}{N} \sum_{m=0}^{N-1} \sum_{n=0}^{N-1} j e^{\frac{j2\pi nm}{N}} \left( \frac{2\pi\epsilon n}{N} + \delta_\Omega \right) m e^{-\frac{j2\pi km}{N}} \\ &+ \frac{1}{N} \sum_{m=0}^{N-1} \sum_{n=0}^{N-1} -\frac{1}{2} e^{\frac{j2\pi nm}{N}} \left( \frac{2\pi\epsilon n}{N} + \delta_\Omega \right)^2 m^2 e^{-\frac{j2\pi km}{N}} \\ &+ \frac{1}{N} \sum_{m=0}^{N-1} \sum_{n=0}^{N-1} -\frac{1}{6} j e^{\frac{j2\pi nm}{N}} \left( \frac{2\pi\epsilon n}{N} + \delta_\Omega \right)^3 m^3 e^{-\frac{j2\pi km}{N}} \end{aligned} \quad (4.14)$$

Using the first term of Eq. 4.14 and setting  $\delta_\Omega$  to zero, the first-order approximation for  $\epsilon$  is obtained.

$$\tilde{S}_{\text{eps}}(k) = \frac{1}{N^2} \sum_{m=0}^{N-1} \sum_{n=0}^{N-1} j 2\pi m n e^{\frac{j2\pi m(n-k)}{N}} \epsilon \quad (4.15)$$

This approximation is for the case where there is frequency skew, but no frequency shift. Since we are interested in the phase change that is induced by the frequency skew effect, the phase of Eq. 4.15 was evaluated for  $\epsilon = 0.01008$  and plotted for a couple of values of  $N$ . This particular  $\epsilon$  value was chosen because it marked the edge of the linear TOA region as shown in Fig. 4.8 from the Matlab simulations. Fig. 4.17 shows the phase response for  $N = 16$ , which appears linear except for a slight curve near the ends. Increasing  $N$  to 128 (Fig. 4.18) causes the curves near the ends to be a bit more pronounced but the phase response is still linear which agrees with the simulation results. Since the phase response of the first-order approximation is linear, the end result is simply that the signal appears to have undergone a time shift. Since the receivers are assumed to be clock synchronized, these RTOA time shifts cancel upon formation of TDOAs. Hence, no distortion of TDOA estimates will result as long as the phase shift remains a linear function of frequency index.

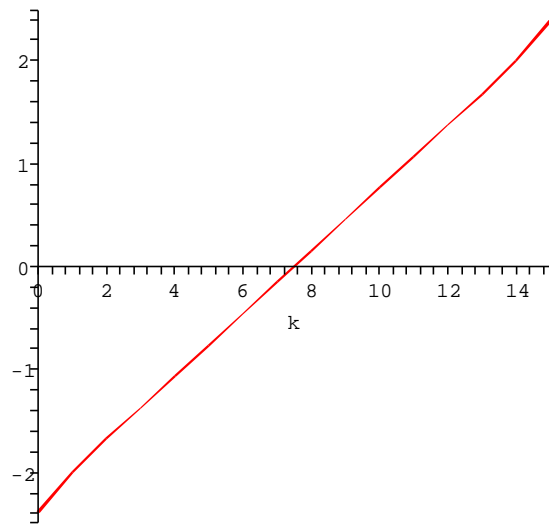


Figure 4.17: Phase response of first order approximation for  $\epsilon = 0.01008$  and  $N = 16$ .

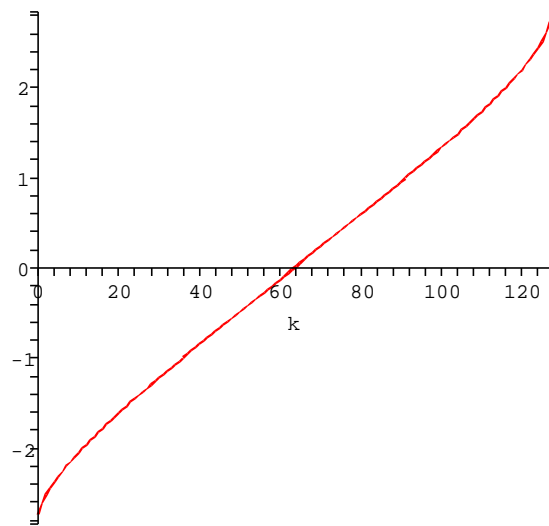


Figure 4.18: Phase response of first order approximation for  $\epsilon = 0.01008$  and  $N = 128$ .

Similarly we can write the first-order approximation for  $\delta_\Omega$  from the first term of Eq. 4.14.

$$\tilde{S}_{\text{delta}}(k) = \frac{1}{N} \sum_{m=0}^{N-1} \sum_{n=0}^{N-1} j m e^{\frac{j2\pi m(n-k)}{N}} \delta_\Omega \quad (4.16)$$

Eq. 4.16 evaluates to zero for any value of  $N$  and  $k$  which shows that the first-order approximation for  $\delta_\Omega$  contributes nothing to the first order approximation. Therefore, any amount of frequency shift has no effect on signal phase to the first order approximation. The second-order and third-order approximations for  $\delta_\Omega$  are also useful to examine.

$$\tilde{S}_{\text{delta}}(k) = -\frac{1}{2N} \sum_{m=0}^{N-1} \sum_{n=0}^{N-1} m^2 e^{\frac{j2\pi m(n-k)}{N}} \delta_\Omega^2 = 0 \quad (4.17)$$

$$\tilde{S}_{\text{delta}}(k) = -\frac{1}{N} \sum_{m=0}^{N-1} \sum_{n=0}^{N-1} \frac{1}{6} j e^{\frac{j2\pi mn}{N}} \delta_\Omega^3 m^3 e^{\frac{-j2\pi km}{N}} = 0 \quad (4.18)$$

Both the second and third order approximations also evaluate analytically to zero for any value of  $N$  and  $k$  which again shows that neither contribute to the second and third order approximations, hence they have no effect on signal phase. Clearly, frequency shift, by itself, has no effect so the next thing to examine is a combination of both frequency skew and shift. Setting  $\delta_\Omega^2$  and  $\epsilon^2$  to zero in the third term of the Taylor expansion (Eq. 4.14) yields the first-order approximation for  $\delta_\Omega$  and  $\epsilon$ .

$$\tilde{S}_{\text{delta,eps}}(k) = -\frac{1}{2N^2} \sum_{m=0}^{N-1} m^2 \sum_{n=0}^{N-1} 4 \left( e^{\frac{j\pi nm}{N}} \right)^2 \epsilon \pi n \delta_\Omega N \left( e^{\frac{j\pi km}{N}} \right)^{-2} \quad (4.19)$$

Again, we are interested in phase change induced by frequency skew and shift effects, therefore the phase of Eq. 4.15 was evaluated for  $\epsilon = 0.01008$  and  $\delta_\Omega = 0.1$  using a couple values of  $N$ . The  $\epsilon$  and  $\delta_\Omega$  values again correspond to the Matlab simulation results in Fig. 4.8. The phase plot for  $N = 16$  (Fig. 4.10) is mostly linear with a slight curve near the end points. Comparing this phase response with that of Fig. 4.8 shows that the non-zero  $\delta_\Omega$  does make this phase response slightly less linear at the end points. This corresponds to the Matlab simulation results that showed frequency shift does degrade TOA performance in the presence of frequency skew. Similar results are seen in Fig. 4.11 where  $N = 128$ . plotted (Fig. 4.20). Since the phase response of the first-order approximation is linear in frequency, the locator system TDOA estimates will again not be deviated by frequency skew.

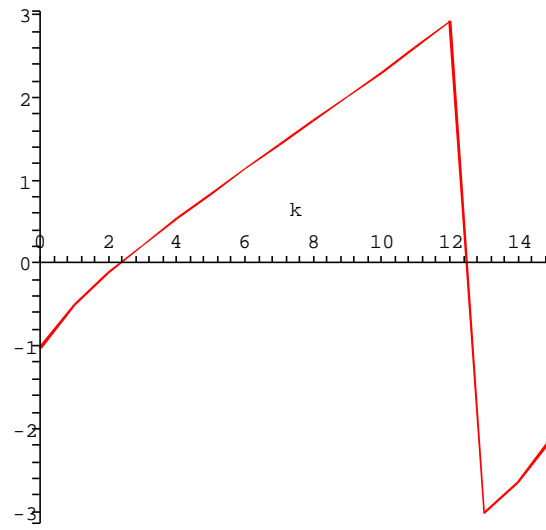


Figure 4.19: Phase response of first order approximation for  $\epsilon = 0.01008$ ,  $\delta_\Omega = 0.1$  and  $N = 16$ .

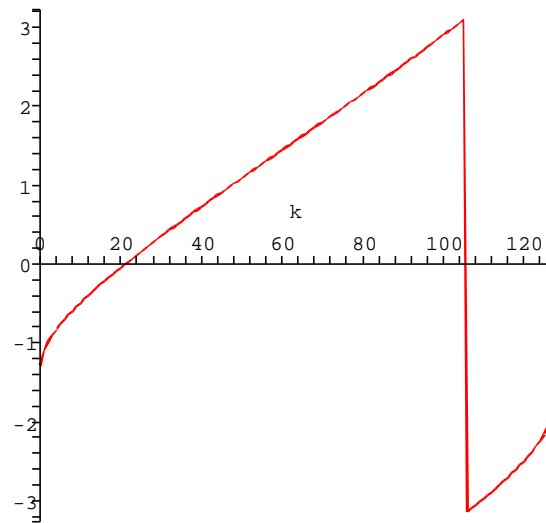


Figure 4.20: Phase response of first order approximation for  $\epsilon = 0.01008$ ,  $\delta_\Omega = 0.1$  and  $N = 128$ .

## 4.4 Experimental Results

The audio demonstrator was used to confirm that the locator would function with moderate amounts of frequency skew and large amounts of frequency shift. This generation of the demonstrator used a baseband audio signal with clock synchronization between transmitter and receivers. Therefore, frequency skew and shift effects are not a problem, so those effects have to be introduced into the transmitted signal using the signal generation function described in Sec. 4.1. Three  $f_{\text{skew}}$  values were tried; 0.99, 0.999 and 0.9999. When  $f_{\text{skew}} = 0.99$ , the locator system completely failed to estimate the location correctly. Reducing the frequency skew to 0.999, allowed the locator to correctly estimate the transmitter location occasionally. Finally, decreasing  $f_{\text{skew}}$  further to 0.9999 allowed the locator to estimate the transmitter location continuously with no noticeable impact on performance. In our simulations an early test was directed towards determining where TOA estimation became non-linear (Fig. 4.6). We saw that that occurred when  $f_{\text{skew}} = 0.9888$  so it was expected that transmitter location estimation, in the demonstrator, wouldn't work for  $f_{\text{skew}} = 0.99$  and  $f_{\text{skew}} = 0.999$  but would work when  $f_{\text{skew}} = 0.9999$  since that is in the linear region. Two different shift values were tried,  $f_{\text{shift}} = 0.01$  and  $f_{\text{shift}} = 0.5$ , with neither giving the locator any difficulty estimating the transmitter location. This result confirmed simulation results where TOA estimation wasn't affected by frequency skew for values smaller than  $\pm 6.1$ . The analytical results showed that frequency skew by itself had no effect at all so the experimental findings were in agreement.

## Chapter 5

# Conclusions

In this work we have discussed our Precision Personnel locator system which uses fixed receivers to locate mobile transmitters in limited area of operations. TOAs and TDOAs were discussed as a means to perform position estimation of the transmitters. TOAs are usable for location only when transmitter and receiver clocks are synchronized. In order to simplify transmitter design as much as possible the location system needs to work without clock synchronization between transmitters and receivers which introduces a time offset in the received signal. Since the transmitter's clock is asynchronous then the TOAs estimated at each receiver are actually RTOAs because the transmitter and receiver don't share the same concept of time. If clock synchronized receivers are assumed then taking the TDOA between RTOAs subtracts out the time offset and the set of TDOAs can be used, along with the receiver locations, for position estimation.

In Chapter 3 RTOA performance estimation, in the context of our locator system, was examined through simulations, analytical predictions and experimental confirmation. A Matlab RTOA performance simulator and simulation process was described. Running the simulation for a specified number of Monte Carlo trials gave us some performance benchmarks for the system error. We were able to use the Matlab simulation results to confirm the analytical performance equations by comparing RTOA estimation variance. Position error equations were derived for specific sensor geometry which resulted in a nomograph relating system energy, fractional bandwidth and sensor array size for a practical sensor ge-

ometry configuration. A design example using the nomograph illustrated how little power is necessary to achieve a useful location accuracy of 1/10 m. Performance measurements using our audio demonstrator system yielded RTOA accuracy of less than 1/10 in. Experimental results were also confirmed against the analytical performance equations using parameters for the audio locator.

A closer look at the effects that asynchronous transmitter clocks have on RTOA estimation was the subject of Chapter 4. Inconsistencies between transmitter and receiver sampling frequencies introduce a frequency skew in the received signal that can severely increase RTOA estimation error. Similarly, local oscillator variations can introduce a frequency shift into the received signal that also can impact RTOA estimation. A function for generating a signal with specified skew and shift effects was used for Matlab simulations. It was found that TOA estimation error is linear in the presence of frequency skew but if enough skew is introduced system response becomes non-linear. Examination of the linear range showed that frequency shift for fixed skew values has some impact on TOA estimation and that its impact increases as signal bandwidth is reduced.

The signal DFT was modeled analytically with skew and shift variables added. A Taylor expansion of the perturbed signal equation allowed skew and shift effects to be studied separately and together. The first three frequency shift terms evaluated to zero which indicates that by itself frequency shift has no effect. On the other hand the first order frequency skew term's phase response was mostly linear with some slight non-linearity near the end points. This effect slowly worsened as DFT length was increased. The phase response for the first order skew and shift term showed that frequency shift does have a relatively small effect when coupled with a frequency skew effect. Frequency skew and shift effects were introduced into the audio demonstrator's signal to confirm the simulation results. Frequency skew in small amounts had no effect on transmitter location but as skew was increased location estimation began to become increasingly erratic before finally failing altogether. Frequency shift didn't have any noticeable impact on transmitter location.

In this thesis we have obtained design formulae and the capacity to accurately simulate any system under consideration. The next steps in the project, which will dwell on the physical realization of high bandwidth, high frequency RF implementation, can now be

conducted with the benefit of proper system engineering. Future analysis and simulation may also be necessary as the additional problems of multi-path degradation and other interfering signals are introduced.

# Bibliography

- [1] BARD, J. D., HAM, F. M., AND JONES, W. L. An Algebraic Solution to the Time Difference of Arrival Equations. In *Southeastcon '96. 'Bringing Together Education, Science and Technology'*, *Proceedings of the IEEE* (April 1996), pp. 313–319.
- [2] BHASKAR RAO, K. A. Model Based Processing of Signals: A State Space Approach. In *Proceedings of the IEEE* (February 1992), pp. 283–309.
- [3] CYGANSKI, D., ORR, J., AND MICHALSON, W. Performance of a Precision Indoor Positioning System Using a Multi-Carrier Approach. In *ION NTM* (Jan. 2004).
- [4] FASAL, J. *Nomography*. Frederick Ungar Publishing Co., New York, 1968.
- [5] INTERNATIONAL CRYSTAL MANUFACTURING CO. *ICM: Precision Crystal FAQs*.
- [6] MANNO, I. *Introduction to the Monte Carlo Method*. Akadémiai Kiadó, Budapest, Hungary, 1999.
- [7] POZAR, D. *Microwave Engineering*, second ed. John Wiley & Sons Inc., New York, 1998.
- [8] WOODACRE, B. TDOA Positioning and TOA-based Calibration for Precision Location. Master's thesis, Worcester Polytechnic Institute, 2004.